OPEN

Cell Death and Differentiation (2015) 22, 921–934

www.nature.com/cdd

Slingshot-Cofilin activation mediates mitochondrial and synaptic dysfunction via Aβ ligation to β1-integrin conformers

This article has been corrected since Advance Online Publication and a corrigendum is also printed in this issue

JA Woo[1,2], X Zhao[1,2], H Khan[2], C Penn[2], X Wang[2,3], A Joly-Amado[2,3], E Weeber[2,3], D Morgan[2,3] and DE Kang[*,1,2]

The accumulation of amyloid-β protein (Aβ) is an early event associated with synaptic and mitochondrial damage in Alzheimer's disease (AD). Recent studies have implicated the filamentous actin (F-actin) severing protein, Cofilin, in synaptic remodeling, mitochondrial dysfunction, and AD pathogenesis. However, whether Cofilin is an essential component of the AD pathogenic process and how Aβ impinges its signals to Cofilin from the neuronal surface are unknown. In this study, we found that Aβ42 oligomers ($A\beta42_O$, amyloid-β protein 1–42 oligomers) bind with high affinity to low or intermediate activation conformers of β1-integrin, resulting in the loss of surface β1-integrin and activation of Cofilin via Slingshot homology-1 (SSH1) activation. Specifically, conditional loss of *β1-integrin* prevented $A\beta42_O$-induced Cofilin activation, and allosteric modulation or activation of β1-integrin significantly reduced $A\beta42_O$ binding to neurons while blocking $A\beta42_O$-induced reactive oxygen species (ROS) production, mitochondrial dysfunction, depletion of F-actin/focal Vinculin, and apoptosis. Cofilin, in turn, was required for $A\beta42_O$-induced loss of cell surface β1-integrin, disruption of F-actin/focal Talin–Vinculin, and depletion of F-actin-associated postsynaptic proteins. SSH1 reduction, which mitigated Cofilin activation, prevented $A\beta42_O$-induced mitochondrial Cofilin translocation and apoptosis, while AD brain mitochondria contained significantly increased activated/oxidized Cofilin. In mechanistic support *in vivo*, AD mouse model (APP (amyloid precursor protein)/PS1) brains contained increased SSH1/Cofilin and decreased SSH1/14-3-3 complexes, indicative of SSH1–Cofilin activation via release of SSH1 from 14-3-3. Finally, genetic reduction in *Cofilin* rescued APP/Aβ-induced synaptic protein loss and gliosis *in vivo* as well as deficits in long-term potentiation (LTP) and contextual memory in APP/PS1 mice. These novel findings therefore implicate the essential involvement of the β1-integrin–SSH1–Cofilin pathway in mitochondrial and synaptic dysfunction in AD.
Cell Death and Differentiation (2015) **22,** 921–934; doi:10.1038/cdd.2015.5; published online 20 February 2015

The defining pathological hallmark of Alzheimer's disease (AD) is the accumulation of amyloid-β protein (Aβ) in brain associated with tau pathology, synapse loss, cytoskeletal aberrations, mitochondrial dysfunction, and cognitive decline. Soluble oligomeric forms of Aβ are thought to be the most toxic species, resulting in synaptic loss and downstream neurotoxicity.[1] An early and consistent impairment secondary to Aβ oligomer treatment in primary neurons is the shrinkage of dendritic spines[2] involving the rearrangement of filamentous actin (F-actin) cytoskeleton in spines and loss of spine-associated proteins such as postsynaptic density-95 (PSD95) and Drebrin,[3,4] as well as impaired mitochondrial function.[5,6] Studies have implicated an involvement of the F-actin-severing protein Cofilin in Aβ-induced dendritic spine changes,[3,4] accumulation of Cofilin–Actin aggregates/rods in AD brains,[7] and increased Cofilin activity in brains of AD patients.[8] Cofilin normally functions as a key regulator of Actin dynamics that destabilizes F-actin. Cofilin is inactivated by phosphorylation on Ser3 by LIM kinase 1 (LIMK1), whereas its dephosphorylation by Slingshot homology-1 (SSH1) activates Cofilin.[9–11] Upon oxidative stress and/or Ca^{2+} elevation,[9,12,13] SSH1 is activated and active Cofilin becomes oxidized on cysteine residues, resulting in rapid mitochondrial translocation to promote mitochondria-mediated apoptosis and induction of Cofilin–Actin pathology.[14,15] Despite the circumstantial evidence for the involvement of Cofilin in AD pathogenesis, no direct evidence thus far has been presented.

Heterodimeric integrins (α- and β-subunits) comprise major adhesion receptors that regulate multiple facets of cellular function, including adhesion, motility, survival, and synaptic plasticity.[16] A primary function of integrins is to link the extracellular matrix to the F-actin cytoskeleton via structural

[1]Department of Molecular Medicine, University of South Florida Morsani College of Medicine, Tampa, FL, USA; [2]USF Health Byrd Alzheimer's Institute, University of South Florida Morsani College of Medicine, Tampa, FL, USA and [3]Molecular Pharmacology and Physiology, University of South Florida Morsani College of Medicine, Tampa, FL, USA
*Corresponding author: DE Kang, Department of Molecular Medicine, USF Health Byrd Alzheimer's Institute, University of South Florida Morsani College of Medicine, 4001 E. Fletcher Avenue-MDC36, Tampa, FL 33613, USA. Tel: +1 858 519 7081; Fax: +1 858 519 7081; E-mail: dkang@health.usf.edu

Abbreviations: Aβ, amyloid-β protein; $A\beta42_O$, amyloid-β protein 1–42 oligomers; AD, Alzheimer's disease; APP, amyloid precursor protein; CHO cells, Chinese Hamster Ovary cells; DIV, days *in vitro*; F-actin, filamentous actin; FC, focal complex; fEPSP, field excitatory postsynaptic potential; FITC, fluorescein isothiocyanate; FN, fibronectin; GFAP, glial fibrillary acidic protein; H2DCF, 2′,7′-dichlorofluorescein; IgG, immunoglobulin G; LTP, long-term potentiation; mGluR5, metabotropic glutamate receptor 5; mRFP, monomeric red fluorescent protein; LIMK1, LIM kinase 1; NOX, NADPH oxidase; PAK1, p21-activated kinase 1; Pir-B, paired immunoglobin-like receptor-B; PrP^c, Prion protein (cellular); PPF, paired pulse facilitation; PSD95, postsynaptic density-95; ROS, reactive oxygen species; SSH1, Slingshot homolog 1; TfR, transferrin receptor

Received 25.9.14; revised 19.11.14; accepted 16.12.14; Edited by N Bazan; published online 20.2.15

scaffolding proteins such as Talin and Vinculin.[17,18] Among several proposed surface Aβ oligomer receptors such as PrP^c (Prion protein (cellular))/mGluR5 (metabotropic glutamate receptor 5)[19,20] and paired immunoglobin-like receptor-B (Pir-B)[8], it has been shown that α2/β1 and αv/β1-integrins are also required to mediate Aβ-induced apoptosis and impairment in LTP.[21,22] However, whether Aβ binds directly to integrins and how Aβ engagement alters downstream integrin function are unknown. In this study, we explored the mechanistic relationships among $A\beta42_O$ (amyloid-β protein 1–42 oligomers), β1-integrin, and Cofilin activities *in vitro*, HT22 cells, primary neurons, and genetically modified mice. Here we show that $A\beta42_O$ exhibits direct high-affinity binding β1-integrin, inducing its conformational alteration, loss of surface β1-integrin, and disruption of integrin-associated focal complexes (FCs), as well as mitochondrial and synaptic dysfunction via a pathway involving ROS-dependent activation of SSH1 and Cofilin.

Results

$A\beta42_O$ induces loss of cell surface β1-integrin but not TfR or PrP^c and reduces β1-integrin activation. We prepared Aβ1-42 oligomers ($A\beta42_O$) as previously characterized.[23] These $A\beta42_O$ preparations contained SDS-resistant dimers, trimers, and tetramers (Supplementary Figure S1A). The indicated $A\beta42_O$ concentrations, heretofore, are based on the monomer concentration. To determine whether $A\beta42_O$ alters surface levels or activation status of β1-integrin, we plated the hippocampus-derived HT22 mouse cell line in the presence and absence of fibronectin (FN) coating, treated them with $A\beta42_O$ for 2 h and performed cell surface biotinylation experiments. Cell surface β1-integrin normalized to total was significantly reduced by ~60% regardless of FN coating after $A\beta42_O$ treatment without altering total β1-integrin, although FN coating also significantly increased surface β1-integrin (Figures 1a and b; and Supplementary Figures S1B and C). Although FN coating modestly, but significantly, increased surface/total transferrin receptor (TfR), $A\beta42_O$ (1 μM) had no significant effect on surface TfR (Figures 1a and c). Surface PrP^c was unaffected by either FN coating or $A\beta42_O$ treatment (Figures 1a and d). In FN-coated coverslips, $A\beta42_O$ (2 h) also significantly reduced total surface β1-integrin levels by ~45% and further reduced activated surface β1-integrin by ~75% as detected by the HUTS-4 antibody[24] in non-permeabilized cells (Figures 1e and f). In days *in vitro* (DIV)-14 fixed and permeabilized neurons, $A\beta42_O$ treatment *per se* significantly reduced the FITC (fluorescein isothiocyanate)-HUTS-4-positive activated β1-integrin by >50%, which was significantly prevented by the β1-integrin allosteric modulating antibody (MAB1965)[25] and the PrP^c function blocking antibody (6D11)[19] (Figures 1g and h).

β1-integrin allosteric modulation or activation reduces $A\beta42_O$ binding to neurons, HT22 cells, and purified β1-integrin. We next assessed $A\beta42_O$ binding to mature DIV21 hippocampal neurons by adding 100 nM FITC-$A\beta42_O$ for 1 h at 37 °C with prior incubation (1 h) with control immunoglobulin G (IgG), MAB1965, or HUTS-4 monoclonal IgGs. As expected, FITC-$A\beta42_O$ associated with dendrites and dendritic spines, and such binding was significantly reduced by MAB1965 IgG by ~50% (Figures 2a and b). The HUTS-4 IgG, which has been shown to enhance ligand binding to β1-integrin,[26] also significantly reduced FITC-$A\beta42_O$ binding to neurons by >60% (Figures 2a and b). As previously shown,[19] 6D11 IgG significantly reduced FITC-$A\beta42_O$ binding to neurons by ~50% (Figures 2a and b). In *β1-integrin fl/fl* neurons (conditional knockout, cKO)[27] transduced with high-titer lentiviruses expressing Cre-monomeric red fluorescent protein (mRFP), FITC-$A\beta42_O$ binding to neurons was significantly reduced by >60% (Figures 2c and d) while reducing β1-integrin expression by ~80–90% (Figure 2e). We next determined whether Aβ binds directly to β1-integrin-Fc (extracellular domain fused with human IgG-Fc).[26] Biotin-$A\beta42_O$ bound to purified β1-integrin-Fc (Figure 2f) coated on ELISA plates with high affinity in the presence of 5 mM $MgCl_2$, which induces an intermediate open integrin conformation (Figure 2g; $K_d = 11.3$ nM based on monomer calculation). In the absence of cation, minimal binding of $A\beta42_O$ to β1-integrin-Fc was detected and did not appreciably increase with increasing biotin-$A\beta42_O$ (Figure 2g). Surprisingly, $MnCl_2$ (0.5 mM), which induces the maximal open activation state of integrins,[26] failed to support $A\beta42_O$ binding to β1-integrin-Fc (Figure 2g), indicating that $A\beta42_O$ prefers an intermediate activation state of β1-integrin. Accordingly, FITC-$A\beta42_O$ binding to HT22 cells was also significantly reduced in the presence of 0.5 mM $MnCl_2$ or MAB1965 but not $MgCl_2$ (Figures 2h and i). Unlike $A\beta42_O$, Aβ42 monomers and fibrils bound poorly to β1-integrin-Fc (Supplementary Figure S2).

Essential role of β1-integrin in $A\beta42_O$-induced cofilin activation and reciprocal requirement of cofilin in $A\beta42_O$-induced depletion of surface β1-integrin and FCs . $A\beta42_O$ (2 h, 1 μM) treatment to primary cortical neurons significantly induced Cofilin dephosphorylation/activation (Figures 3a and b). However, such Cofilin dephosphorylation was absent in β1-integrin cKO neurons transduced with Lenti-Cre-mRFP (Figures 2a and b). We next determined whether Cofilin *per se* is also required for the observed $A\beta42_O$-induced depletion of cell surface β1-integrin in HT22 cells. $A\beta42_O$ reduced surface β1-integrin, and Cofilin siRNA reduced Cofilin levels (Figure 3c). However, Cofilin siRNA increased surface β1-integrin levels and prevented the $A\beta42_O$-induced reduction in surface β1-integrin (Figure 3c). Quantification of surface β1-integrin and PrP^c levels secondary to Cofilin siRNA demonstrated that Cofilin knockdown significantly increases the surface/total β1-integrin ratio without affecting surface/total PrP^c ratio (Figures 3d and e), similar to that observed with $A\beta42_O$ treatment.

A direct consequence of β1-integrin internalization is the disruption of integrin and F-actin-associated FCs, structurally organized by Talin and Vinculin. We treated DIV14 cortical neurons or HT22 cells with or without $A\beta42_O$ (1 μM) and subjected them to sequential extraction of the cytosolic fraction on ice with the surfactant saponin, followed by extraction of membrane and cytoskeletal elements with SDS sample buffer (FC-enriched fraction). $A\beta42_O$ saliently reduced FC-enriched but not cytosolic (cyto) Vinculin and Talin in

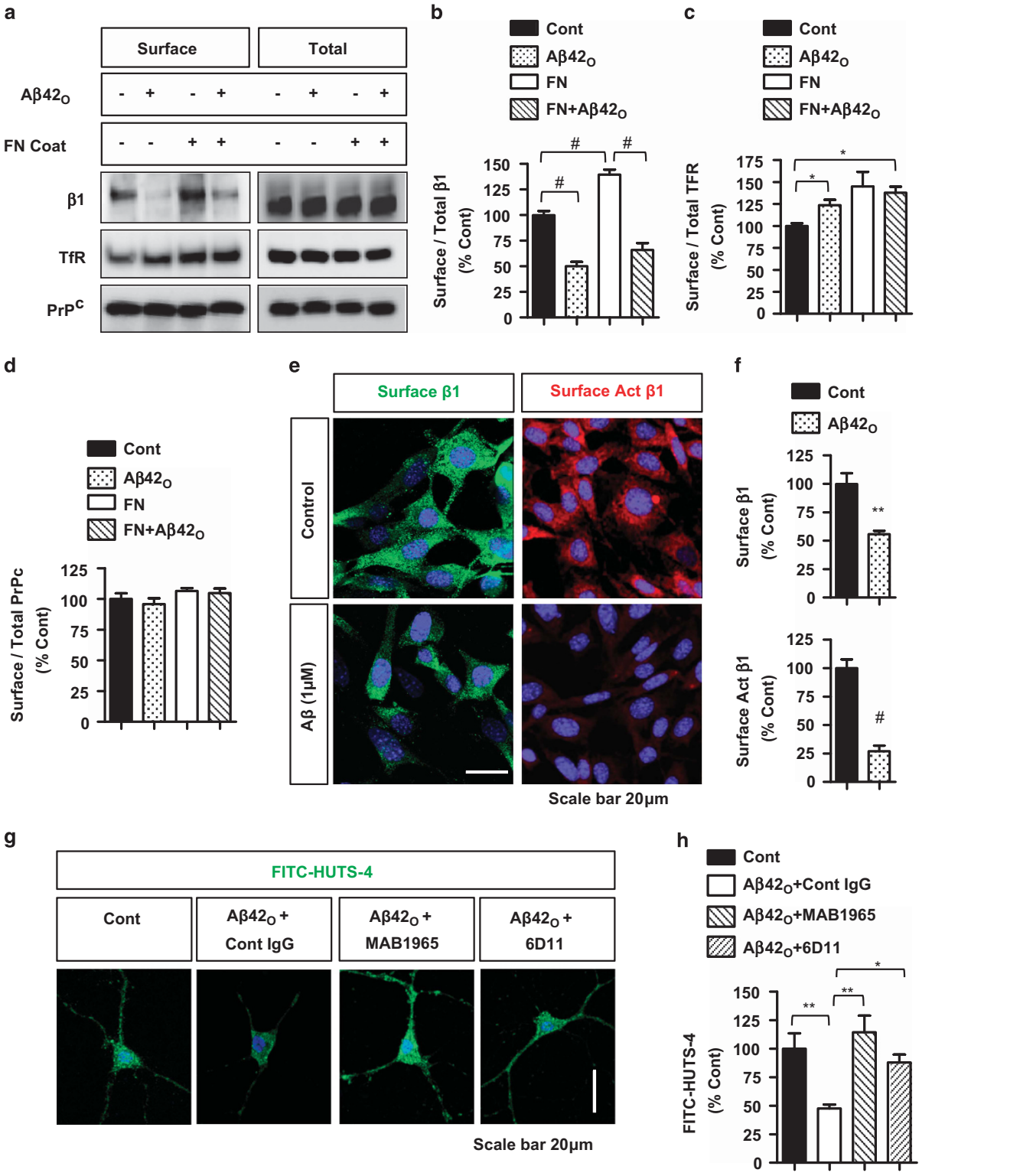

Figure 1 Aβ42O induces loss of cell surface β1-integrin but not TfR or PrP^C and reduces β1-integrin activation. (**a**–**d**) HT22 cells plated with/without FN, treated with/without Aβ42O (1 μM, 2 h), subjected to surface biotinylation (surface), and direct immunoblotting (total) or immunoprecipitation for biotin (surface) and immunoblotting for the indicated proteins. (**b**–**d**) Quantification of normalized surface/total β1, TfR, and PrP^C ($n \geqslant 3$ replicates, ANOVA, *post hoc* Tukey, $^*P < 0.05$, $^\#P < 0.0005$). Error bar represent S.E.M. (**e** and **f**) HT22 cells treated with /without Aβ42O and immunostained for total surface β1-integrin or activated surface β1-integrin (HUTS-4 antibody) without membrane permeabilization ($n \geqslant 4$ replicates, *T*-test, $^{**}P < 0.005$, $^\#P < 0.0005$). (**g** and **h**) Direct staining for activated β1-integrin (FITC-HUTS-4 antibody) in fixed and permeabilized DIV14 primary hippocampal neurons after treatment with/without Aβ42O (1 μM, 2 h) and/or control ascites IgG (1 : 250), MAB1965 (1 : 250), or 6D11 (1 : 50). (**h**) Quantification of FITC-HUTS-4 immunoreactivity ($n = 4$ replicates, ANOVA, *post hoc* Tukey, $^*P < 0.05$, $^{**}P < 0.005$)

primary neurons (Supplementary Figure S3A) and HT22 cells (Supplementary Figures S3B and C). To observe focal Vinculin in a different way, we cultured primary hippocampal neurons to DIV21 and treated them with or without Aβ42$_O$ for 2 h followed by staining for Vinculin and F-actin. Regardless of Aβ42$_O$ treatment, Vinculin nearly completely co-localized with F-actin, and discrete puncta positive for both Vinculin and F-actin were seen in dendritic spines (Figure 3f). However,

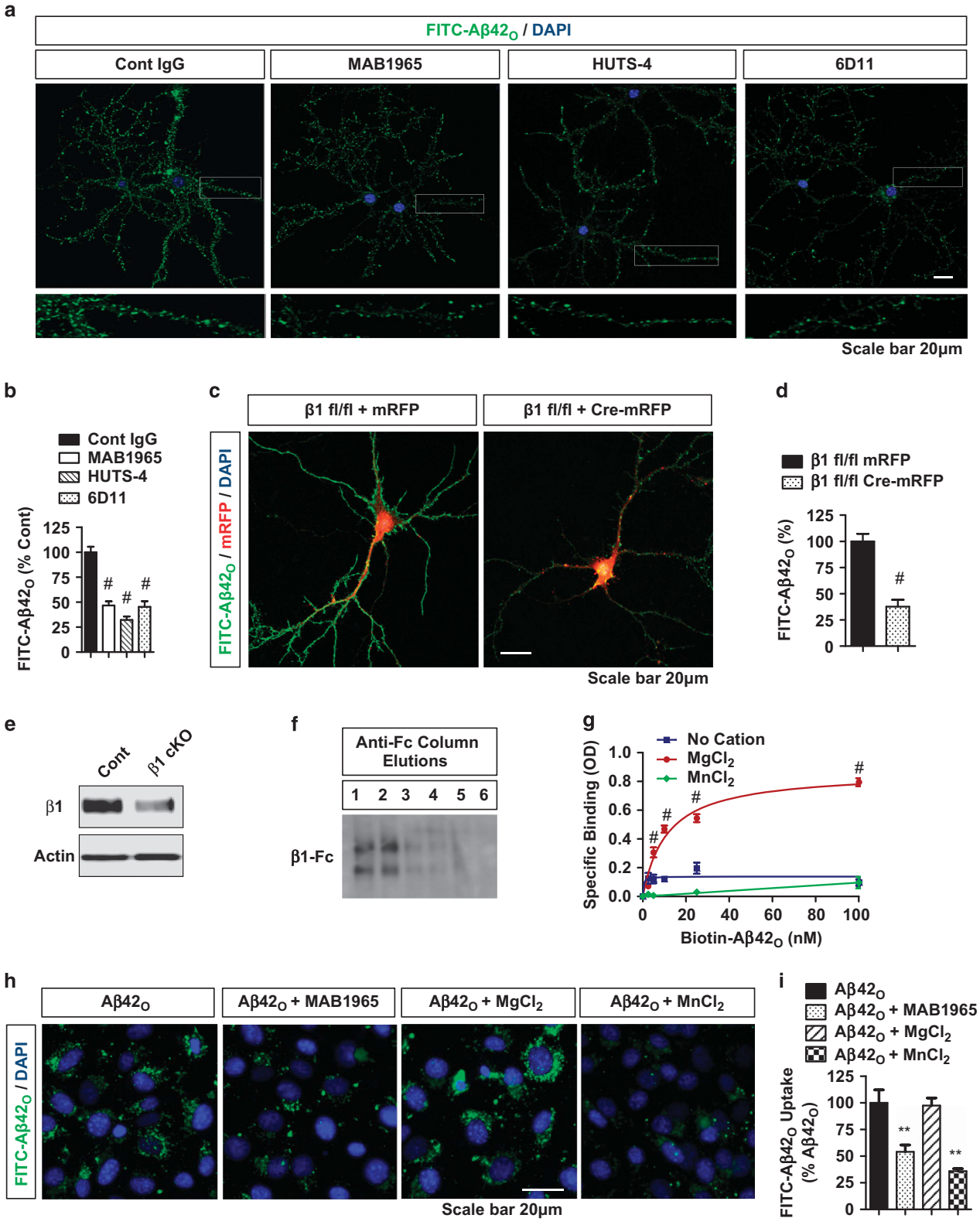

Aβ42$_O$ exposure significantly reduced focal Vinculin immunoreactivity in spine-containing dendrites after subtracting the diffuse cytosolic stain in dendrites (Figures 3f and g). In 7-month wild-type (WT) mice, Vinculin immunoreactivity in the CA3 pyramidal neurons demonstrated punctate immunoreactivity throughout neuronal cell bodies, indicative of FCs, with little diffuse staining. However, in 7-month-old APP/PS1 transgenic littermates,[28] Vinculin immunoreactivity appeared markedly more diffuse and cytosolic in the CA3 pyramidal neurons (Supplementary Figure S3D), with significant 75% and ~50% reductions in area and size of focal Vinculin, respectively, in APP/PS1 mice compared with WT littermates (Supplementary Figure S3E).

Aβ42$_O$ treatment (1 μM) to WT neurons depleted focal Vinculin and Talin (Figure 3h). However, the same treatment in littermate *Cofilin*$^{+/-}$ neurons did not significantly deplete Vinculin and Talin in the FC-enriched fraction compared with WT neurons (Figures 3h and i). Accordingly, Cofilin knockdown also prevented Aβ42$_O$-induced depletion of focal Vinculin in HT22 cells (Supplementary Figures S4A and B). Next, we stereotaxically injected 8-month-old APP/PS1 mice hippocampi with 2 μl β1-integrin allosteric modulating/neutralizing antibody (MAB1965 prediluted 1 : 10) into the right hemisphere and control IgG (control ascites fluid prediluted 1 : 10) into the left hemisphere. Forty-eight hours post injection, MAB1965 IgG significantly increased focal Vinculin area and size in CA3 pyramidal neurons compared with control IgG in the contralateral hemisphere (Figures 3j and k), indicating that endogenous β1-integrin mediates APP/Aβ-induced depletion of focal Vinculin in brain.

Essential roles of cofilin and β1-integrin in Aβ42$_O$-induced depletion of F-actin and F-actin-associated synaptic proteins in primary hippocampal neurons. The primary function of Cofilin is to sever F-actin, which promotes synaptic remodeling via accelerating Actin dynamics.[29] As Aβ42$_O$ induced Cofilin activation, we cultured hippocampal neurons derived from *Cofilin*$^{+/-}$ and WT littermate mice and cultured them to DIV21. Aβ42$_O$ (1 μM, 2 h) significantly depleted F-actin, Drebrin, and PSD95 in dendritic spines and spine-containing neurites of WT neurons (Figures 4a and b). However, the same Aβ42$_O$ treatment had no significant effects in *Cofilin*$^{+/-}$ neurons (Figures 4a and b), indicating that a critical threshold of endogenous Cofilin is required for Aβ42$_O$-induced depletion of F-actin, Drebrin, and PSD95. Likewise, allosteric modulation of β1-integrin with MAB1965 IgG completely prevented the depletion of F-actin and PSD95 induced by Aβ42$_O$ (Figures 4c and d), indicating that the β1-integrin-Cofilin pathway mediates Aβ42$_O$-induced changes in F-actin and F-actin-associated postsynaptic proteins.

Requirement of SSH1 in Aβ42$_O$-induced cofilin translocation to mitochondria and accumulation of mitochondrial cofilin in AD brains. Activated and oxidized Cofilin is known to translocate to mitochondria, where it induces mitochondrial dysfunction.[13,14] We treated HT22 cells with or without Aβ42$_O$ (1 μM) for 0, 2, and 4 h and fractionated intact mitochondria from cytosol. Aβ42$_O$ rapidly increased the translocation of Cofilin to mitochondria, while decreasing phospho-Cofilin in the cytosol (Figures 5a and b). No phospho-Cofilin was detected in the mitochondrial fraction (Figure 5a), consistent with its activation requirement for translocation. RNAi-mediated knockdown of SSH1, the phosphatase that activates Cofilin,[10] significantly prevented Aβ42$_O$-induced translocation of Cofilin to mitochondria together with increased Cofilin phosphorylation (Figure 5c), indicating that Aβ42$_O$ activates and promotes Cofilin translocation to mitochondria via SSH1. We next isolated mitochondria from the frontal cortex of age-matched cognitively normal control and AD patients (Supplementary Figure S5). In the absence of DTT in sample buffer (non-reducing), we detected cysteine-oxidized Cofilin monomers, dimers, trimers, and higher-order oligomers, which essentially all collapsed to the monomer form in the presence of DTT (reducing; Figure 5d). This banding pattern is similar to that observed from Cofilin–Actin rods, which also require activation and oxidation-induced disulfide bonding to form.[15] Total Cofilin (all four bands in non-reducing condition), oxidized Cofilin oligomers (dimers or larger), and Cofilin monomers were significantly increased in mitochondria of AD (Figures 4d and e), results that fulfill the prediction from cultured cells, and suggest that activated and oxidized mitochondrial Cofilin has a pathogenic role in AD.

Aβ42$_O$-induced ROS production, mitochondrial dysfunction, and apoptosis via the β1-integrin–SSH1–Cofilin activation pathway. HT22 cells were treated with Aβ42$_O$ (1 μM) with or without vehicle, NADPH oxidase (NOX) inhibitor, HUTS-4 IgG, or MAB1965 IgG and then subjected to live-cell imaging for JC-1, Mitosox-Red, and H2DCF (2′,7′-dichlorofluorescein). As expected, Aβ42$_O$ treatment (1 μM, 2 h) significantly decreased mitochondrial membrane potential (increased JC-1 green/red ratio), increased mitochondrial superoxide (Mitosox-Red), and increased ROS levels

Figure 2 β1-Integrin allosteric modulation or activation reduces Aβ42$_O$ binding to neurons, HT22 cells, and purified β1-integrin as effectively as the loss of β1-integrin (**a** and **b**) FITC-Aβ42$_O$ (100 nM, 1 h) binding to DIV21 primary hippocampal neurons with/without prior treatment (1 h) of control IgG, MAB1965 (β1-integrin allosteric modulator, 1 : 250), HUTS-4 (β1-integrin allosteric activator, 1 : 250), and/or 6D11 (PrP^c blocking, 1 : 50) monoclonal antibodies. Bottom panel magnified from regions of white rectangles. (**b**) Quantification of FITC-Aβ42$_O$ binding ($n \geqslant 5$ replicates, ANOVA, *post hoc* Tukey, $^{\#}P < 0.0005$ compared with control IgG). Error bars represent S.E.M. (**c**–**e**) FITC-Aβ42$_O$ (100 nM, 1 h) binding to *β1-integrin fl/fl* neurons transduced with Lenti-mRFP (cont) or Lenti-Cre-mRFP (β1 cKO). (**d**) Quantification of FITC-Aβ42$_O$ binding ($n = 5$ replicates, *T*-test, $^{\#}P < 0.0005$). (**e**) Representative blots of β1-integrin from cKO (Lenti-Cre-mRFP) *versus* cont (Lenti-mRFP) neurons (all neurons including nontransduced). (**f**) Conditioned medium from CHO cells transfected with β1-integrin-Fc affinity purified with anti-Fc affinity column, sequentially eluted, and immunoblotted with anti-Fc. (**g**) Purified β1-integrin-Fc from fractions 1 and 2 captured by 96-well plates coated with anti-Fc IgG, subjected to biotin-Aβ42$_O$ binding and/or incubated with different cations ($MgCl_2$, 5 mM and $MnCl_2$, 0.5 mM). (**h**) $K_d = 10.3$ nM with $MgCl_2$. Two-way ANOVA *post hoc* Bonferroni, $n = 4$ replicates, $^{\#}P < 0.0005$. (**h** and **i**) HT22 cells treated with FITC-Aβ42$_O$ (0.1 μM, 2 h) and/or β1-integrin blocking IgG (MAB1965, 1 : 500), $MnCl_2$ (0.5 mM), or $MgCl_2$ (5 mM), and subjected fluorescence microscopy. (**h**) Representative images of FITC-Aβ42$_O$ binding/uptake show inhibition by MAB1965 antibody and $MnCl_2$. (**i**) Quantification of mean intensities of FITC-Aβ42$_O$ binding/uptake ($n = 4$ replicates, ANOVA, *post hoc* Tukey, $^{**}P < 0.005$ compared with FITC-Aβ42$_O$ alone)

(H2DCF; Figures 6a and b; and Supplementary Figure S6A). However, co-incubation with HUTS-4, MAB1965, or NOX inhibitor significantly prevented such changes induced by Aβ42$_O$, although the JC-1 membrane potential measure was not fully restored by these treatments (Figures 6a and b and Supplementary Figure S6A). Accordingly, MAB1965 significantly prevented Aβ42$_O$-induced apoptosis in primary neurons and HT22 cells as assessed by Annexin V/PI staining (Supplementary Figures S6B and D). Similarly, Annexin V/PI staining also demonstrated significant induction of early

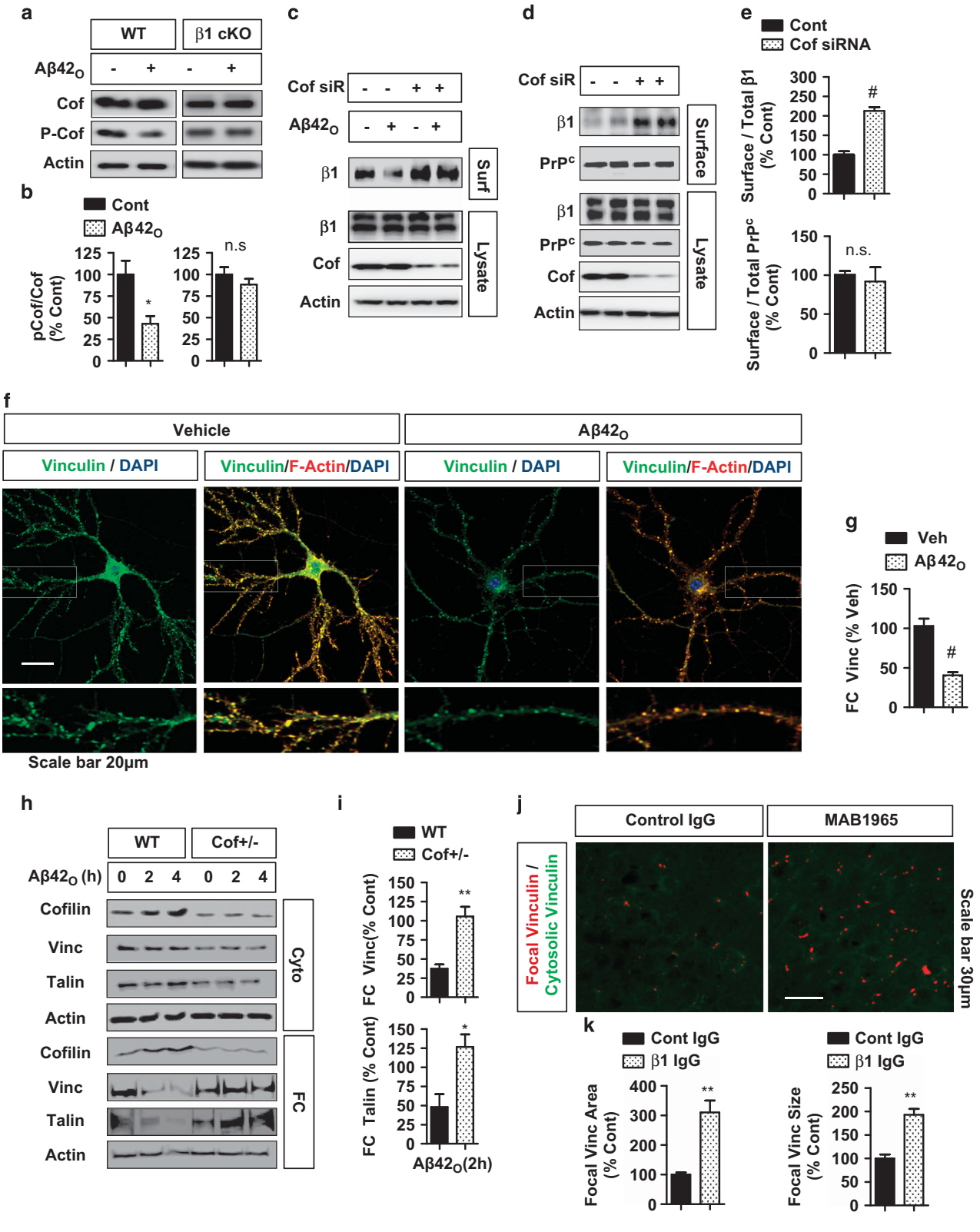

(Annexin V) and late (PI) apoptosis after 24 h Aβ42$_O$ (1 μM) treatment, which was nearly completely blocked by SSH1 siRNA knockdown (Figures 6c and d), indicating that SSH1-dependent Cofilin activation is required for Aβ42$_O$-induced apoptosis.

A key mechanism of Cofilin regulation is via the binding of SSH1 to 14-3-3, which renders SSH1 sequestered in an inactive state. However, the oxidation of 14-3-3 releases SSH1, thereby leading to SSH1 activation.[12,30] In 7-month-old APP/PS1 mice, SSH1/Cofilin complexes and 14-3-3/SSH1 complexes were significantly increased and decreased, respectively, compared with WT littermate mice (Figures 6e and f), indicating the release of SSH1 from 14-3-3 and association of SSH1 with Cofilin in APP/PS1 mice. Accordingly, phospho-Cofilin was significantly decreased in APP/PS1 mice, despite no apparent changes in total 14-3-3, SSH1, or Cofilin in TX-100 solubilized extracts

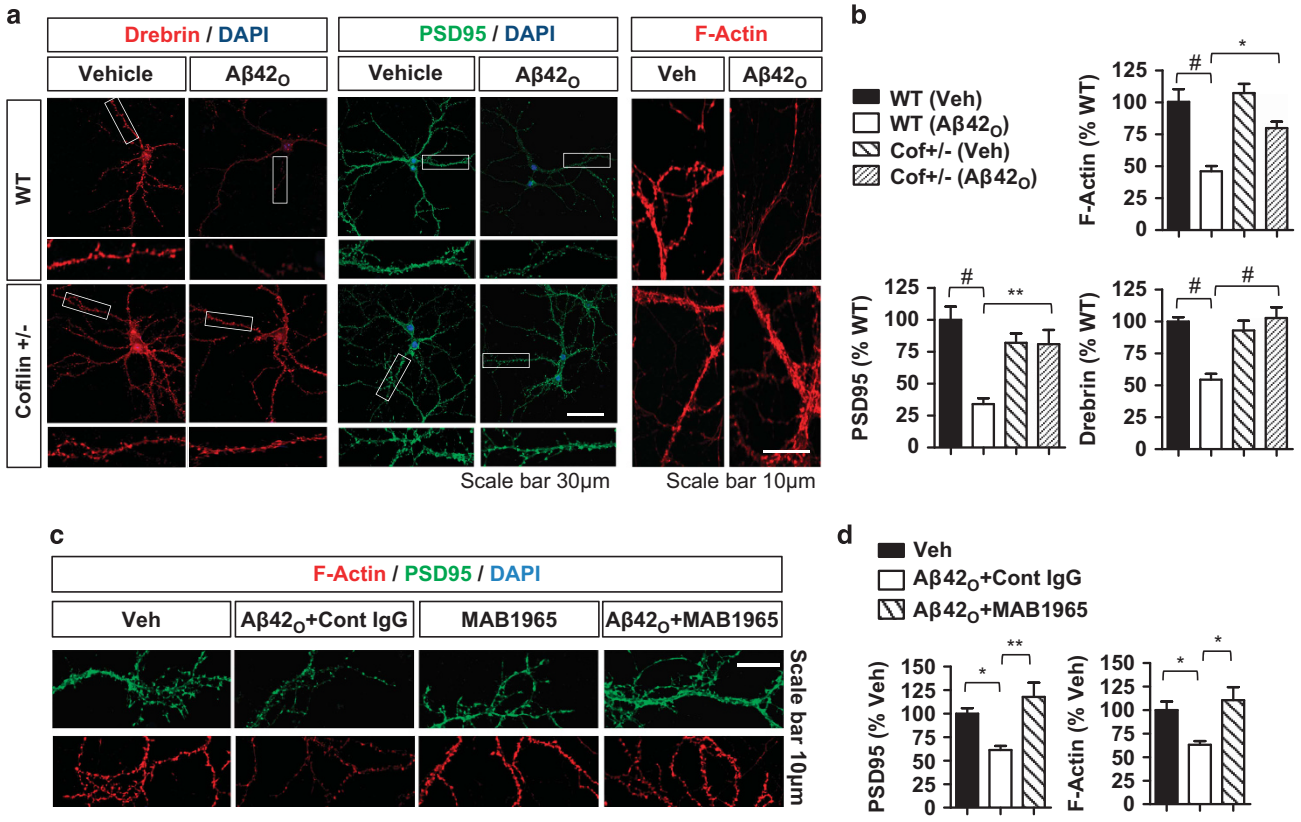

Figure 4 Essential roles of Cofilin and β1-integrin in Aβ42$_O$-induced depletion of F-actin and associated synaptic proteins in primary hippocampal neurons. (**a** and **b**) WT and *Cofilin*$^{+/-}$ DIV21 hippocampal neurons treated with/without Aβ42$_O$ (1 μM, 2 h) and stained for F-actin (rhodamine-phalloidin), Drebrin, or PSD95. (**b**) Quantification of mean intensities of Drebrin, PSD95, and F-actin in spine-containing neurites ($n=4$–6 replicates, ANOVA, *post hoc* Tukey, $^*P<0.05$, $^{**}P<0.005$, $^{\#}P<0.0005$). Error bars represent S.E.M. (**c** and **d**) DIV21 hippocampal neurons treated with/without Aβ42$_O$ (1 μM, 2 h) and/or control IgG or β1-integrin IgG (MAB1965) and stained for PSD95 and F-actin (rhodamine-phalloidin). (**c**) Representative images showing depletion of PSD95 and F-actin after Aβ42$_O$ treatment, which is prevented by MAB1965. (**d**) Quantification of mean PSD95 and F-actin intensities in spine-containing neurites ($n\geqslant 6$ replicates, ANOVA, *post hoc* Tukey, $^*P<0.05$, $^{**}P<0.005$)

Figure 3 Essential role of β1-integrin in Aβ42$_O$-induced Cofilin activation as well as reciprocal requirement of Cofilin in Aβ42$_O$-induced depletion of surface β1-integrin and F-actin-associated FCs (Vinculin and Talin). (**a** and **b**) DIV14 cortical WT or β1-integrin cKO neurons (transduced with Lenti-Cre) treated with/without Aβ42$_O$ (1 μM, 2 h) and subjected to immunoblotting. Note the decrease in p-Cofilin by Aβ42$_O$ in WT but not in β1 cKO neurons ($n=4$ replicates, *T*-test, $^*P<0.05$). Error bars represent S.E.M. (**c**) HT22 cells transfected with control or Cofilin siRNA, treated with Aβ42$_o$ (1 μM, 2 h) and subjected cell surface biotinylation followed by direct immunoblotting or IP with anti-biotin and immunoblotting. Note that Cofilin knockdown prevents Aβ42$_O$-induced depletion of surface β1-integrin. (**d** and **e**) HT22 cells transfected with control or Cofilin siRNA and subjected to cell surface biotinylation followed by direct immunoblotting or IP with anti-biotin and immunoblotting. (**d**) A representative experiment showing a dramatic increase in surface β1-integrin but no change in surface PrP^c after Cofilin knockdown. (**e**) Quantification of β1-integrin normalized to total β1-integrin and surface PrP^c normalized to total PrP^c ($n=4$ replicates, *T*-test, $^{\#}P<0.0005$). (**f** and **g**) DIV21 hippocampal primary neurons treated with/without Aβ42$_O$ (1 μM, 2 h) and subjected to staining for Vinculin, F-actin (rhodamine-phalloidin), and DAPI. Note the near complete co-localization of Vinculin with F-actin, particularly in dendritic spines and loss of Vinculin immunoreactivity with Aβ42$_O$ treatment. (**g**) Quantification of focal Vinculin mean intensity (FC Vinculin) in dendrites and dendritic spines after subtracting the mean diffuse cytosolic intensity in dendrites ($n=5$ replicates, *T*-test, $^{\#}P<0.0005$). Error bars represent S.E.M. (**h** and **i**) DIV14 cortical WT and *Cofilin*$^{+/-}$ neurons treated with/without Aβ42$_O$ (1 μM), subjected to separation of cytosol and FC-enriched fractions followed by immunoblotting. (**h**) Representative blots showing Aβ42$_O$-induced depletion FC Vinculin and Talin in WT but not in *Cofilin*$^{+/-}$ neurons. (**i**) Quantification of FC Vinculin and Talin after 2 h Aβ42$_O$ treatment normalized to respective vehicle treated controls at 100%. ($n=3$ replicates, *T*-test, $^*P<0.05$, $^{**}P<0.01$). (**j** and **k**) Eight-month-old APP/PS1 transgenic mice and their nontransgenic littermates (WT) stereotaxically injected with 2 μl β1-integrin blocking antibody (MAB1965, diluted 1 : 10) into the left hippocampus and 2 μl control IgG (control ascites fluid, diluted 1 : 10) into the right hippocampus and subjected to immunohistochemistry for Vinculin 48 h post injection. (**j**) Representative images of Vinculin FCs (red) in the CA3 of the hemisphere injected with β1-integrin blocking antibody compared with the control IgG injected contralateral hemisphere. Focal Vinculin threshold adjusted to convert highest intensity signals from green to red puncta without altering diffuse cytosolic signal. (**k**) Quantification of focal Vinculin area and size normalized to control IgG ($n=5$ mice, 2 M and 3 F, *T*-test, $^{**}P<0.005$)

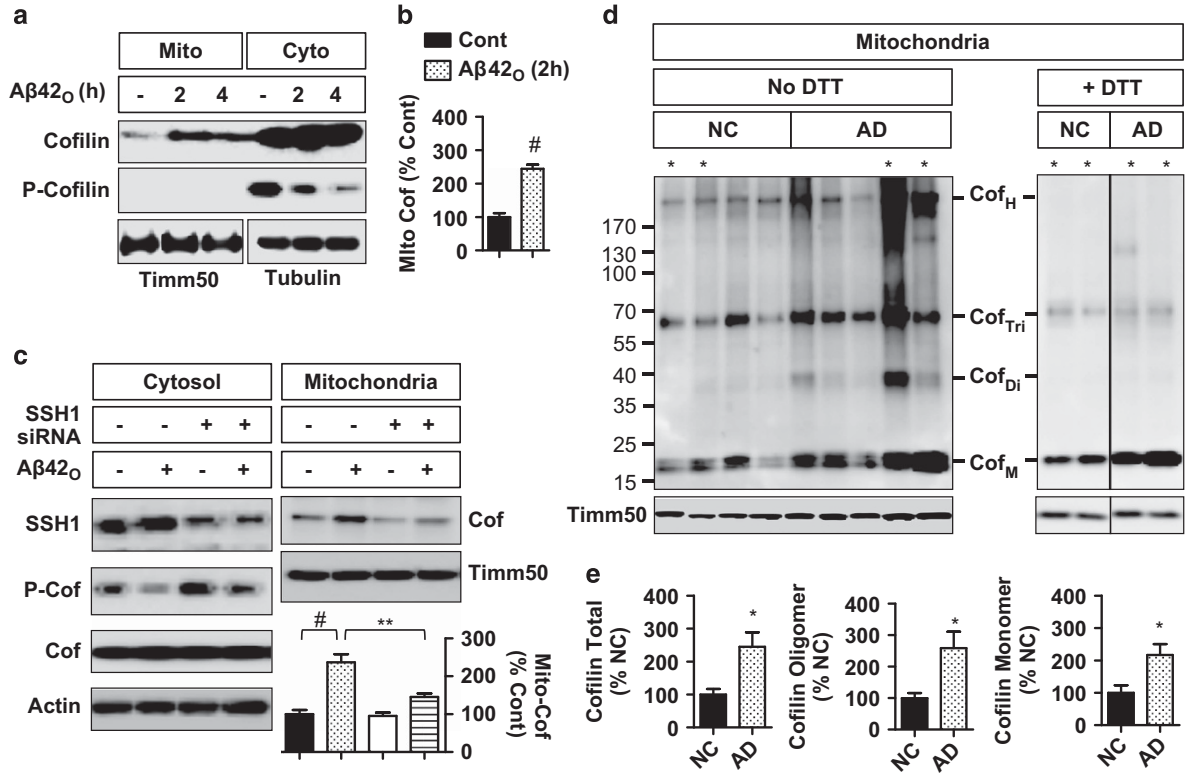

Figure 5 Requirement of Slingshot-1 (SSH1) in Aβ42$_O$-induced Cofilin translocation to mitochondria and accumulation of mitochondrial Cofilin in AD brains. (**a** and **b**) HT22 cells treated with/without Aβ42$_O$ (1 μM) for the indicated times and subjected to separation of mitochondria and cytosol fractions followed by immunoblotting for the indicated proteins. (**a**) Representative blots showing Cofilin dephosphorylation (cytosol) and translocation to mitochondria (mito) after Aβ42$_O$ treatment. (**b**) Quantification of cytosolic and mitochondrial Cofilin ($n=4$ replicates, *T*-test, $^{**}P<0.005$, $^{\#}P<0.0005$). (**c**) HT22 cells transfected with control or SSH1 siRNA, treated with/without Aβ42$_O$ (1 μM, 4 h), and subjected to separation of cytosol *versus* mitochondria followed by immunoblotting for the indicated proteins. Note that SSH1 siRNA prevents Aβ42$_O$-induced Cofilin dephosphorylation and translocation to mitochondria ($n=4$ replicates, ANOVA, *post hoc* Tukey, $^{\#}P<0.0005$). (**d** and **e**) Mitochondria isolated from mid-frontal cortex of AD ($n=5$) and cognitively NC ($n=4$) and immunoblotted for Cofilin and Timm50 with or without DTT in sample buffer. (**d**) Representative blots showing abundance of Cofilin monomers (Cof$_M$), dimers (Cof$_{Di}$), trimers (Cof$_{Tri}$), and high molecular weight species (Cof$_H$) in AD (blot on left run without DTT). Samples with asterisk (*) run with DTT and boiling show reduction of oxidized Cofilin oligomers to collapsed monomers (blot on right). (**e**) Quantification of Cofilin total (all four Cofilin bands), oligomers (Cof$_{Di}$, Cof$_{Tri}$, and Cof$_H$), and monomers (Cof$_M$) (*T*-test, $^{*}P<0.03$)

(Figures 6e and f). Aβ42$_O$ treatment also reduced 14-3-3/SSH1 complexes in HT22 cells, which was largely restored with prior treatment with MAB1965 or the potent anti-oxidant Trolox (Supplementary Figure S7B). Likewise, Aβ42$_O$ treatment significantly increased SSH1/Cofilin complexes in HT22 cells (Supplementary Figures S7C and D). These results therefore demonstrate that APP/Aβ promotes Cofilin activation at least in part via the β1-integrin-ROS-14-3-3/SSH1 pathway.

Cofilin reduction rescues app/aβ-induced gliosis and loss of synaptic proteins, as well as LTP and contextual memory deficits in APP/PS1 mice. We examined brains of 7-month-old APP/PS1, APP/PS1;*Cofilin*$^{+/-}$, and WT littermate mice for neurodegenerative phenotypes, including glial fibrillary acidic protein (GFAP) for astrogliosis as well as PSD95 (postsynaptic) and Synapsin I (presynaptic) for synaptic integrity. As expected, APP/PS1 mouse hippocampi demonstrated significantly increased GFAP immunoreactivity throughout the hippocampus as well as diminished Synapsin I and PSD95 immunoreactivity within the stratum lucidium (synaptic terminating zone) of CA3 (Figures 7a and b). In contrast, APP/PS1;*Cofilin*$^{+/-}$ mice showed significantly reduced GFAP immunoreactivity and increased Synapsin I and PSD95 immunoreactivities compared with APP/PS1 littermate mice, essentially indistinguishable from WT littermates (Figures 7a and b).

We next tested short-term and long-term synaptic plasticity from acute hippocampal slices prepared from 3-month-old WT, APP/PS1, and APP/PS1;*Cofilin*$^{+/-}$ mice. The stimulating electrode was placed in the Schaffer collaterals of the hippocampus, and the recording electrode was positioned at the CA1 stratum radiatum below the pyramidal cell layer. As shown in Figures 7c, the input–output curves did not markedly differ among WT, APP/PS1, and *APP/PS1;Cofilin*$^{+/-}$ slices. In paired pulse facilitation (PPF) experiments, we observed significant differences in fEPSP slope across genotypes among all interstimulus intervals (Figure 7d). However, correction for multiple comparisons showed that only APP/PS1;*Cofilin*$^{+/-}$ and WT slices differed significantly at the 40-ms interstimulus interval (Figure 7d). For LTP measurements, we detected no differences in fEPSP slope among WT, APP/PS1, and APP/PS1;*Cofilin*$^{+/-}$ slices at baseline (Figure 7e). However, after theta burst stimulation (TBS), we observed significant differences in fEPSP slope across genotypes for all time points (Figure 7e). Correction for multiple comparisons showed that APP/PS1 slices were significantly impaired in

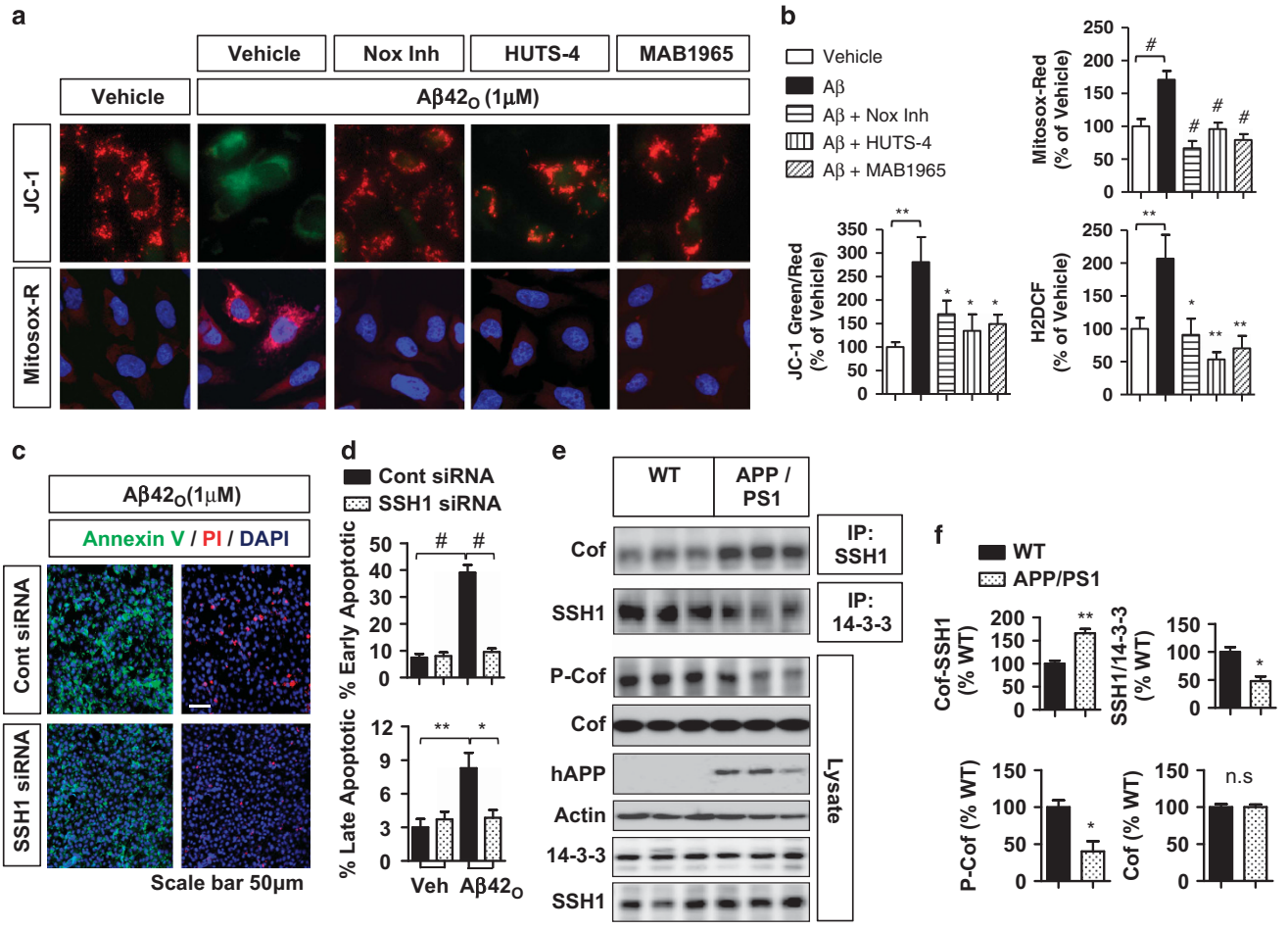

Figure 6 Aβ42$_O$-induced ROS production, mitochondrial dysfunction, and apoptosis via the β1-integrin–SSH1–Cofilin activation pathway. (**a** and **b**) HT22 cells treated with vehicle or Aβ42$_O$ (1 μM) for 2 h with or without 1 h prior treatment with Nox inhibitor (VAS2870, 40 nM), HUTS-4 (β1-integrin allosteric activating IgG, 1 : 250), or MAB1965 (β1-integrin allosteric modulating IgG, 1 : 250) and subjected to live-cell imaging for JC-1 (mitochondrial membrane potential, green/red ratio), Mitosox-Red (mitochondrial superoxide indicator), or H2DCF (general ROS indicator). Note that β1-integrin conformational modulation or inhibition of Nox significantly reduces Aβ42$_O$-induced mitochondrial dysfunction and overall ROS increase. Representative H2DCF images are shown in Supplementary Figure S6A. (**b**) Quantification of JC-1 green/red ratio, Mitosox-Red, and H2DCF intensities ($n=6$, 1-way ANOVA, *post hoc* Tukey, $^*P<0.05$, $^{**}P<0.01$, or $^{\#}P<0.005$ compared with Aβ42$_O$. (**c** and **d**) HT22 cells transiently transfected with control or SSH1 siRNA, treated with / without Aβ42$_O$ (1 μM, 18 h) in 1% FBS medium, and subjected to FITC Annexin V/propidium iodide (PI) staining and fluorescence confocal microscopy. (**c**) Representative images showing reduction in Annexin V (early apoptosis) and PI (late apoptosis) staining in cells transfected with SSH1 siRNA (with Aβ42$_O$). (**d**) Quantification of Annexin V/PI staining ($n=4$ replicates, ANOVA, *post hoc* Tukey, $^*P<0.05$, $^{**}P<0.005$, $^{\#}P<0.0005$). (**e** and **f**) Seven-month-old WT and APP/PS1 littermate mouse frontal cortex homogenates (1% Triton X-100) immunoprecipitated for pan-14-3-3 or SSH1 and immunoblotted for SSH1 or Cofilin. Same brain samples also directly immunoblotted for the indicated proteins. (**e**) Representative blots showing decreased 14-3-3/SSH1 complex and increased SSH1/Cofilin complex in APP/PS1 mice. (**f**) Quantification of SSH1/14-3-3 complex, Cofilin/SSH1 complex, p-Cofilin, and total Cofilin ($n=4$ mice/genotype, 2 M and 2 F, *T*-test, $^*P<0.02$, $^{**}P<0.005$)

fEPSP slope compared with WT and APP/PS1;*Cofilin*$^{+/-}$ slices at every time point up to 1 h, indicating that Cofilin reduction rescues the deficits in LTP in APP/PS1 mice.

We carried out fear conditioning tests (contextual and cued), in which 7-month-old WT, APP/PS1, and APP/PS1;*Cofilin*$^{+/-}$ mice were trained on day 1 for both. On day 2, we tested mice for contextual and cued conditioning memory. We observed no significant differences between the genotypes in percent time spent freezing during the training phase (Figure 7f). However, we observed significant differences across genotypes in the percentage of time spent freezing during the hippocampus-dependent contextual fear conditioning test on day 2. Correction for multiple comparisons showed that WT and APP/PS1;*Cofilin*$^{+/-}$ mice significantly spend more time freezing than APP/PS1 mice (Figure 7g). On the hippocampus-independent cued fear conditioning test, we did not observe significant differences in the percentage of time spent freezing times across genotypes (Figure 7h). We also did not find significant differences among the three genotypes in the rotarod or open-field (total distance traveled and total time spent immobile) tests (Figures 7i–k), indicating the absence of salient perturbations in generalized motor activity or coordination. Taken together, these results demonstrate that endogenous Cofilin is required to mediate the APP/PS1-induced deficits in synaptic plasticity as well as hippocampus-dependent contextual memory but not cued memory.

Discussion

Molecular pathways that govern the production and neurotoxicity of Aβ are attractive therapeutic targets for AD. Although previous studies have shown Cofilin activation in AD brains

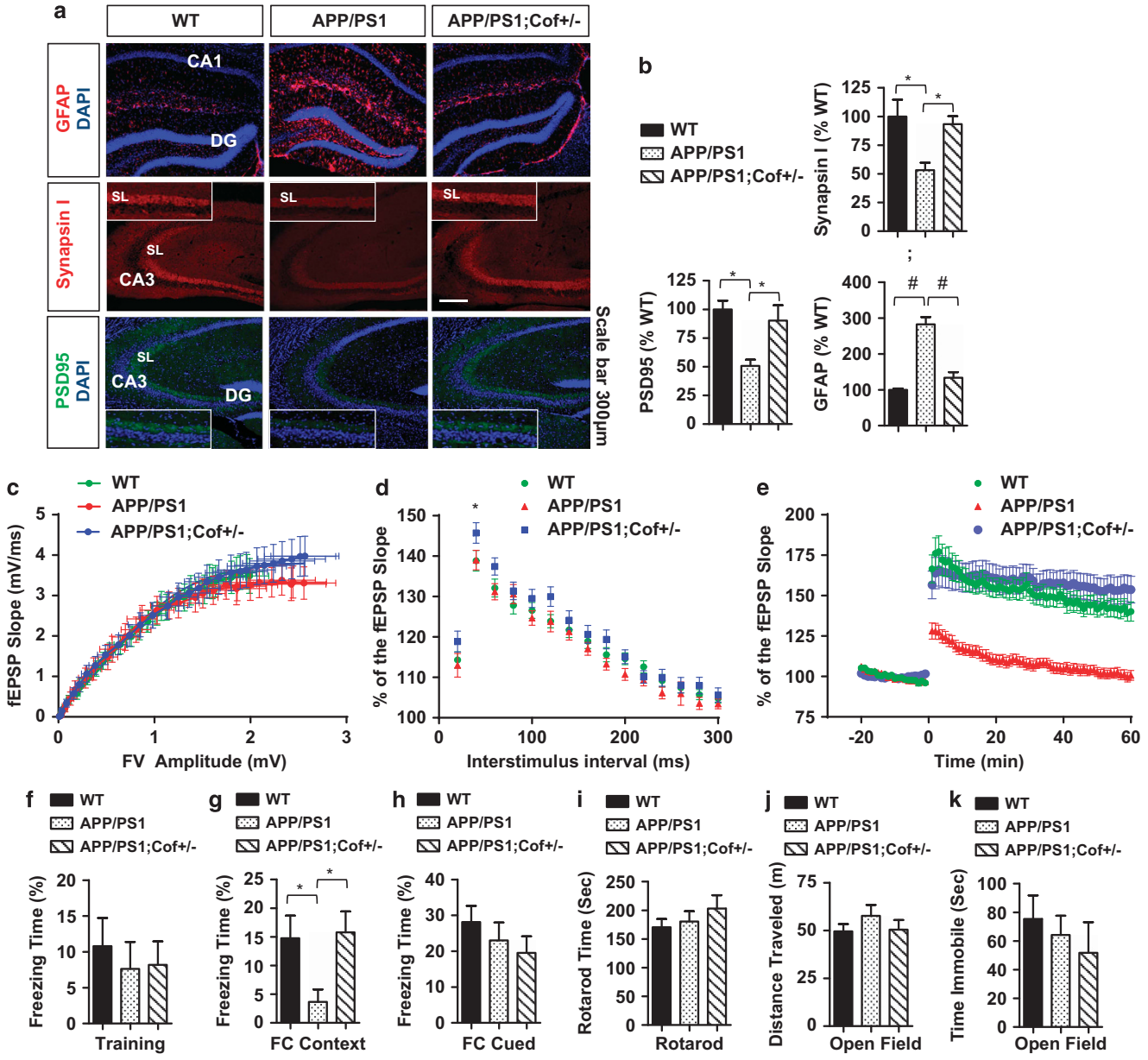

Figure 7 Cofilin reduction rescues APP/Aβ-induced gliosis and loss of synaptic proteins as well as LTP and contextual memory deficits in APP/PS1 mice. (**a** and **b**) Seven-month-old WT, APP/PS1, and APP/PS1;*Cofilin*$^{+/-}$ mice immunostained for GFAP, Synapsin I, and PSD95. (**a**) Representative images showing that Cofilin reduction ameliorates astrogliosis and synaptic damage associated with APP/PS1 mice. (**b**–**d**) Quantification of mean PSD95 and Synapsin I intensities in the stratum lucidum (SL) ($n=4$ mice/genotype, 2 F and 2 M, ANOVA, *post hoc* Tukey, $^{*}P<0.05$, $^{\#}P<0.0005$). (**c**–**e**) Stimulating electrode placed in the Schaffer collaterals of the hippocampus and recording glass electrode positioned at the CA1 stratum radiatum below the pyramidal cell layer. (**c**) Input/output analysis generated by stepping up stimulation amplitude from 1 to 15mV in WT, APP/PS1, and APP/PS1;*Cofilin*$^{+/-}$ acute slices. No significant differences observed ($n=24$ slices from four mice, APP/PS1: 19 slices from four mice, APP/PS1;*Cofilin*$^{+/-}$: $n=20$ slices from three mice). (**d**) PPF showing no significant differences across genotypes and interstimulus interval except between APP/PS1;*Cofilin*$^{+/-}$ and WT slices at the 40-ms interstimulus interval (two-way ANOVA, *post hoc* Bonferroni, $^{*}P<0.05$; WT: $n=32$ slices from four mice, APP/PS1: $n=31$ slices from four mice, APP/PS1;*Cofilin*$^{+/-}$: $n=25$ slices from three mice). (**e**) LTP induced by the TBS showing significant differences in fEPSP slope in APP/PS1 compared with WT and APP/PS1;*Cofilin*$^{+/-}$ slices (two-way ANOVA, *post hoc* Bonferroni, $P<0.0001$ at all time points). (WT: $n=28$ slices from four mice, APP/PS1: $n=33$ slices from four mice, APP/PS1;*Cofilin*$^{+/-}$: $n=20$ slices from three mice). Error bars represent S.E.M. (**f**) Percentage of time spent freezing during training period on day 1 (no significant differences observed by one-way ANOVA or Kruskal–Wallis statistic; WT $n=12$, APP/PS1 $n=8$, APP/PS1;*Cofilin*$^{+/-}$ $n=6$; equal distribution of gender). Error bars represent S.E.M. (**g**) Percentage of time spend freezing during contextual fear conditioning (FC) on day 2 (Kruskal–Wallis statistic = 9.66, $P=0.008$, genotypes = 3, values = 26; *post hoc* Dunn's, $^{*}P<0.05$; WT $n=12$, APP/PS1 $n=8$, APP/PS1;*Cofilin*$^{+/-}$ $n=6$; equalized distribution of gender). (**h**) Percentage of time spent freezing during cued fear conditioning (FC) freezing on day 2 (no significant differences observed by one-way ANOVA or Kruskal–Wallis statistic; WT $n=12$, APP/PS1 $n=8$, APP/PS1;*Cofilin*$^{+/-}$ $n=6$; equalized distribution of gender). (**i**) Total time spent on rotarod test (no significant differences observed by one-way ANOVA or Kruskal–Wallis statistic; WT $n=11$, APP/PS1 $n=7$, APP/PS1;*Cofilin*$^{+/-}$ $n=5$; equalized distribution of gender). (**j**) Total distance traveled during open-field test (no significant differences observed by one-way ANOVA or Kruskal–Wallis statistic; WT $n=11$, APP/PS1 $n=7$, APP/PS1;*Cofilin*$^{+/-}$ $n=5$; equalized distribution of gender). (**k**) Total time spent immobile during open-field test (no significant differences observed by 1-way ANOVA or Kruskal–Wallis statistic; WT $n=11$, APP/PS1 $n=7$, APP/PS1;*Cofilin*$^{+/-}$ $n=5$; equalized distribution of gender)

and potential involvement of β1-integrin in Aβ-induced apoptosis,[7,8,21,22] it was unknown whether endogenous Cofilin *per se* and different β1-integrin conformers are required for molecular events leading to $A\beta42_O$-induced neurodegeneration and how the β1-integrin–Cofilin signaling pathway mediates AD-relevant pathogenic processes.

In this study, we demonstrated for the first time that $A\beta42_O$ induces the depletion of surface β1-integrin via its direct binding to low-intermediate activation conformers of β1-integrin, as detected by competition of $A\beta42_O$ binding to neurons and HT22 cells with the β1-integrin activating antibody (HUTS-4) or $MnCl_2$, both of which induce high conformational activation of β1-integrin.[24,26] Moreover, $MnCl_2$ essentially eliminated $A\beta42_O$ binding to purified β1-integrin-Fc. However, $A\beta42_O$ did not bind to β1-integrin-Fc in the absence of Mg^{2+}, suggesting that an intermediate/partially open conformation of integrin is required for binding. Although physiological ligands bind with high affinity to the highly active/open conformation of β1-integrin,[26] the human Ecovirus binds to the relatively inactive/closed integrin conformer,[31] similar to what we observed with $A\beta42_O$. This finding raises the intriguing possibility of blocking $A\beta42_O$-induced neurotoxic actions by conformational β1-integrin activation without compromising integrin function. In addition to preferentially binding to low-intermediate activation β1-integrin conformers, $A\beta42_O$ also increased the propensity of β1-integrin to assume a lower-activation conformation, probably by preventing bound β1-integrin from assuming a high-activation state. As $A\beta42_O$ reduced surface β1-integrin levels regardless of FN plating, $A\beta42_O$ likely does not compete with most physiological ligands (i.e., FN) for integrin binding, as seen by its preference for binding to lower-activation conformation of β1-integrin. Although we focused on β1-integrin in this study, it is well known that β1-integrin functions in concert with various α-integrin subunits, such as α2 and αv, which have been shown to be involved in Aβ neurotoxicity,[21] as well as α6, which has been implicated in microglial phagocytosis of fibrillar Aβ together with β1.[32]

Our observation that the PrP^c blocking antibody (6D11) significantly prevented $A\beta42_O$-induced reduction in β1-integrin activation was somewhat surprising. However, it has been reported that PrP^c and Pir-B, both of which bind $A\beta42_O$, negatively regulate β1-integrin activation and signaling,[33,34] raising the possibility that loss of these receptors can also interfere with $A\beta42_O$ binding to β1-integrin in neurons. These receptors, including β1-integrin are typically clustered in pre- and postsynaptic membranes, and their activities are regulated by cross talk at multiple points of convergence by other transmembrane receptors. For example, PrP^c-dependent activation of Fyn requires integrin engagement,[35] and glutamate signaling via NMDARs and AMPARs depends on various Integrin heterodimers.[16] Indeed, β1-integrin is also enriched in dendritic spines and is required for dendrite arborization, maintenance of synapses, and LTP.[36–39] In view of these observations, it is plausible that integrins operate physically and/or functionally in concert with other $A\beta42_O$-binding receptors to mediate $A\beta42_O$ binding and neurotoxicity.

Deletion of β1-integrin resulted in the failure of $A\beta42_O$ to activate Cofilin. At the same time, Cofilin was also required for removal of surface β1-integrin, indicating that Cofilin normally has a role in the trafficking and/or internalization of β1-integrin. As such, we focused on β1-integrin and F-actin-associated structural focal components (Talin/Vinculin) and postsynaptic proteins known to function in concert with F-actin and synaptic remodeling, because the direct consequence of β1-integrin internalization is the disruption of the structural components of FCs (Talin and Vinculin), which anchor the cytoplasmic tail of β1-integrin to F-actin. Thus, it is likely that the F-actin severing activity of Cofilin is responsible for the removal of β1-integrin from the cell surface and the depletion of focal Talin/Vinculin by destabilizing or reducing the F-actin linkage to β1-integrin, changes which were directly analogous to F-actin *per se* and F-actin-regulated postsynaptic proteins (Drebrin and PSD95).

Cofilin activity is associated with dendritic spine growth and shrinkage during LTP and LTD, respectively,[40–42] and Cofilin regulates the trafficking of AMPA receptors in dendritic spines.[43] Therefore, $A\beta42_O$-induced Cofilin activation and resultant F-actin severing/depolymerization also likely underlies the reduction in F-actin and synaptic proteins (PSD95 and Drebrin), both of which could be antagonized by Cofilin reduction or β1-integrin allosteric modulation. β-Arrestin 2 recruits Cofilin to dendritic spines upon NMDA receptor activation to control the remodeling of spines, and β-Arrestin 2 knockout neurons are resistant to Aβ-induced dendritic spine loss through spatial control of Cofilin activation.[44] Likewise, $Cofilin^{+/-}$ neurons were resistant to Aβ-induced depletion of postsynaptic proteins. In view of these observations, it is plausible that Cofilin reduction prevents the sustained over-activation of Cofilin by Aβ oligomers to mitigate the loss of postsynaptic proteins and the deficits in LTP.

Our findings indicated that $A\beta42_O$-induced and β1-dependent Cofilin activation, mitochondrial dysfunction, and apoptosis require endogenous SSH1 at least in part via ROS and 14-3-3. This is consistent with the induction of ROS production by NOX via Rac1-mediated signaling downstream of integrin,[45] $A\beta42_O$–induced Cofilin–Actin pathology via a NOX/PrP^c-dependent manner,[46] activation of SSH1 by oxidation of 14-3-3,[12] Aβ-induced oxidation of 14-3-3,[47,48] and Cofilin-dependent mitochondrial dysfunction downstream of oxidative stress.[13] Although a recent study reported that fibrillar Aβ42 can activate LIMK1 via p21-activated kinase 1, they also observed increased Cofilin dephosphorylation; therefore, Aβ oligomers and fibrils may impact the Cofilin activation pathway via similar but also divergent mechanisms.[49] In addition to ROS-dependent activation of SSH1, it is likely that $A\beta42_O$ can also activate Cofilin via a mechanism involving an increase in cytosolic Ca^{2+}, which in part may be mediated by the PrP^c-mGluR5 complex,[20] as Calcineurin dephosphorylates and activates SSH1.[50] We have also shown that RanBP9, which activates Cofilin, also impairs mitochondrial Ca^{2+} buffering and mitochondrial homeostasis in a Cofilin-dependent manner.[13,51,52]

In summary, our findings indicate that a molecular pathway involving SSH1–Cofilin activation via direct engagement of lower-activation conformers of β1-integrin is essential for both $A\beta42_O$-induced mitochondrial and synaptic dysfunction in AD. Therefore, promoting β1-integrin activation and/or inhibiting excessive Cofilin activation (i.e., SSH1 inhibition) represent potentially viable and novel therapeutic strategies to combat AD pathogenesis.

Materials and Methods

Cells, cDNA constructs, siRNA sequences, and transfections. Hippocampus-derived HT22 and CHO (Chinese Hamster Ovary) 7WD10 cells were maintained in DMEM containing 10% FBS. HT22 and CHO7WD10 cell lines were obtained from Professor David Schubert (Salk Institute, San Diego) and Professor Edward Koo (UC, San Diego). Green fluorescent protein–Vinculin construct was obtained from Professor Ballestrem (University of Manchester, UK).[53] The β1-Fc integrin construct was obtained from Dr. Mould at the University of Manchester (UK). The β1-integrin-Fc construct encodes residues 1-708 (β1 extracellular region) fused in-frame to the hinge regions and CH2 and CH3 domains of human IgGγ1.[26] RNAi sequences targeting Cofilin (5′-GGAGGACCUGGUGUUCAUC-3′) and SSH1 (5′-GAGGAGCUGUCCCGAUGAC-3′) were obtained from GE Dharmacon (Lafayette, CO, USA). All cells were transfected for 48 h using lipofectamine 2000 (Invitrogen, Carlsbad, CA, USA) according to the manufacturer's instructions with either cDNA expression constructs, empty vector controls, siRNA duplexes, or control single-stranded denatured control siRNAs before performing biochemical and/or immunocytochemical assays. All siRNAs were transfected at a final concentration of 100 nM. Cortical and hippocampal primary neurons were derived from postnatal day 0 (P0) pups and grown on Poly-D-lysine-coated coverslips or plates as previously described.[51]

Antibodies and reagents. Antibodies to APP (6E10, Covance, Princeton, NJ, USA), sAPPα (IBL-America, Minneapolis, MN, USA), sAPPβ (IBL-America), β1-integrin (M-106, Santa Cruz Biotechnology, Dallas, TX, USA), activated β1-integrin (HUTS-4, EMD Millipore, Billerica, MA, USA), allosteric β1-integrin neutralizing (MAB1965, EMD Millipore), 6D11 (Santa Cruz), Talin (H-300, Santa Cruz Biotechnology), Vinculin (hVIN-1, Sigma-Aldrich, St. Louis, MO, USA), Cofilin (D3F9, Cell Signaling, Danvers, MA, USA), phospho-Cofilin (77G2, Cell Signaling), SSH1 (SP1711, ECM Biosciences, Versailles, KY, USA), pan-14-3-3- (Santa Cruz Biotechnology), Actin (AC-74, Sigma-Aldrich), Tubulin (TU-02, Santa Cruz Biotechnology), Aβ (D5XD2, Cell Signaling), biotin (B7653, Sigma-Aldrich), GFAP (Invitrogen), Synapsin I (Invitrogen), PSD95 (Abcam, Cambridge, MA, USA), Drebrin (Abcam), MAP2 (EMD Millipore), HRP-linked secondary antibodies (Jackson ImmunoResearch, West Grove, PA, USA), and fluorescently labeled secondary antibodies (Invitrogen) were obtained from the indicated sources. The mouse monoclonal anti-RanBP9 antibody was a generous gift from Professor Elizabetta Bianchi (Pasteur Institute, France). Trolox (Cayman, Ann Arbor, MI, USA), JC-1 (Invitrogen), Mitosox-Red (Invitrogen), H2DCF (Invitrogen), NOX inhibitor III (EMD Millipore) were purchased from the indicated sources. Synthetic Aβ1-42 and FITC-Aβ1-42, and biotin-Aβ1-42 peptides were purchased from American Peptide (Sunnyvale, CA, USA). Aβ1-42 oligomers and fibrils were prepared precisely as previously characterized.[23] Briefly, Aβ1-42 powder was dissolved in HFIP at 1 mM for 30 min at room temperature, aliquoted to Eppendorf tubes, allowed to evaporate overnight in fume hood, and subjected to speed vacuum for 1 h to remove traces of HFIP or moisture. To prepare Aβ oligomers, Aβ1-42 film was then dissolved in DMSO (5 mM), and F-12 cell culture medium (without phenol) was added to a final concentration of 100 μM Aβ1-42 and incubated at 4 °C for 24 h.

Cell/tissue lysis and immunoblotting. Cultured cells or brain homogenates were lysed with lysis buffer (50 mM Tris-Cl, 150 mM NaCl, 2 mM EDTA, and 1% Triton X-100) unless stated otherwise. For separation of cytosolic *versus* focal adhesion-enriched (F) fractions, cytosolic proteins were first released with saponin buffer (0.1% saponin, 25 mM HEPES, and 75 mM potassium acetate) for 10 min on ice followed by extraction of remaining proteins by 2× SDS sample buffer and sonication.[54,55] For isolation of mitochondria, mitochondrial isolation kit (Thermo Scientific, Rockford, IL, USA) was used according to the manufacturer's instructions for cultured cells. Protein quantification was performed by a colorimetric detection reagent (BCA protein assay, Pierce, Rockford, IL, USA). Equal amounts of protein were subjected to SDS-PAGE and transferred to nitrocellulose membranes for immunoblotting. After probing with the primary antibody, the corresponding peroxidase-conjugated secondary antibody was detected by ECL western blot reagents (Pierce). ECL images were captured by the Fuji LAS-4000 imager (LAS-4000, Pittsburgh, PA, USA) and quantified using the ImageJ software (NIH ImageJ, Bethesda, MD, USA).

Cell surface biotinylation assay. Surface biotinylation assays were performed as we previously documented.[56] Briefly, confluent cells in six-well plates were washed three times in phosphate-buffered saline (PBS) and treated with 2.0 mg/ml sulfo-NHS-LC-biotin in PBS, pH 8.0 under gentle shaking for 1 h on ice. The cells were then washed three times in PBS and lysed in 1% Triton X-100 lysis buffer. Biotinylated proteins were isolated by pulldown with anti-biotin antibody together with anti-mouse agarose beads (American Qualex, San Clemente, CA, USA). APP (6E10, Covance) and β1-integrin (M-106, Santa Cruz Biotechnology) within anti-biotin immune complexes were detected by immunoblotting with the indicated antibodies.

Annexin V/PI apoptosis assay. To examine the stage of apoptotic cells, measurements were carried out using FACS Calibur (BD Bioscience, San Jose, CA, USA) or fluorescence microscopy. Cells were either trypsinized/collected stained in solution or directly stained on glass coverslips with Annexin V-fluorescein and PI for 20 min at 25 °C in the dark state using the FITC Annexin V apoptosis detection kit I (BD, San Diego, CA, USA). After washing with ice-cold PBS, cells were measured by flow cytometry or by fluorescence microscopy as previously described.[51]

FITC-Aβ1-42 oligomer binding to primary neurons and HT22 cells. DIV21 hippocampal neurons or HT22 cells were incubated with FITC-A$\beta42_O$ (100 nM) for 1–2 h. Cells were then washed extensively with PBS, fixed with 4% paraformaldehyde, stained with DAPI, and fluorescent images were acquired using the Olympus FV10i confocal microscope (Olympus Corp., Tokyo, Japan). All comparison images were acquired with identical laser intensity, exposure time, and filter. Adjustments to the brightness/contrast were applied equally to all comparison images.

Purification of β1-integrin-Fc and binding to A$\beta42_O$. CHO cells in 10cm plates were transfected with 12 μg β1-integrin-Fc constructs for 48 h. Conditioned medium was collected for 24 h thereafter and spun for 5 min at 1000 × *g*. Proteins in expressed in conditioned medium were captured by the anti-Fc affinity column and eluted by several rounds. Ninety-six-well plates were coated with goat anti-human-Fc at a concentration of 5 μg/ml in DPBS (50 μl per well) for 16 h. Wells were washed with DPBS (100 μl per well) and then blocked for 1 h with 100 μl of 5% (w/v) bovine serum albumin (BSA), 150 mM NaCl, 0.05% (w/v) NaN_3, and 25 mM Tris-Cl, pH 7.4 (blocking buffer). The blocking solution was removed, and wells were then washed three times with 100 μl of 150 mM NaCl and 25 mM Tris-Cl, pH 7.4, and containing 1 mg/ml BSA (washing buffer). Purified β1-Fc was added to the plate incubated at room temperature for 1 h. Wells were washed three times in washing buffer, and biotin-labeled Aβ1-42 (50 μl, monomer, oligomer, or fibrils at the indicated concentrations) were added for 1 h at 37 °C. After washing wells three times in washing buffer, streptavidin-HRP (1 : 2000 dilution in washing buffer, Cell Signaling) was added (50 μl per well) for 30 min at room temperature. Wells were washed four times in washing buffer, and color was developed using the TMB substrate (Cell Signaling) and read at 450 nM wavelength. Background Aβ binding to conditioned medium from mock-transfected CHO cells was subtracted from all measurements (specific binding).

Mice and human samples. APP/PS1, WT, *Cofilin*$^{+/-}$, and β1-integrin fl/fl mice were all bred in the C57BL6 background for at least three generations before interbreeding with each other. APP/PS1 mice were obtained from Jackson Laboratory (Ben Harbor, ME, USA).[28] We generated *Cofilin*$^{+/-}$ knockout mice from an embryonic stem cell gene trap clone originally made by Lexicon Genetics (Woodlands, TX, USA) and deposited into the MMRRC repository (UC, Davis). *Cofilin*$^{+/-}$ mouse brains exhibited ~50% reduction in endogenous Cofilin protein in both hippocampus and cortex compared with littermate WT mice (Supplementary Figure S8). Although *Cofilin*$^{+/-}$ mice were viable and fertile with no salient abnormalities, *Cofilin*$^{+/-}$ × *Cofilin*$^{+/-}$ crosses yielded no viable *Cofilin*$^{-/-}$ pups (embryonic lethal). Detailed genotypic and phenotypic information about these mice are available (http://www.informatics.jax.org/external/ko/lexicon/2682.html). Information on β1-integrin *fl/fl* mice are also available (http://jaxmice.jax.org/strain/004605.html). Postmortem brain samples were obtained from the UC, Irvine, ADRC. Ages, gender, and PMI are indicated in Supplementary Figure S5.

Immunofluorescence. Immunohistochemistry and immunocytochemistry were performed as previously described.[51] Briefly, animals were perfused with 4% paraformaldehyde in PBS, and the brains were post fixed in the same fixative for 24 h. The brains were then cryoprotected in 30% sucrose and sectioned (30 μm) on a cryostat or microtome. For primary neurons and HT22 cells, cells were fixed in 4% paraformaldehyde for 15 min at room temperature. For cell surface protein detection only, Triton X-100 was omitted. After blocking with normal goat serum, primary antibodies were applied overnight at 4 °C, and secondary antibodies were applied for 45 min at room temperature, followed by counterstaining with Hoechst33342 or

DAPI. Immunoreactivities were quantitated from every 12th serial section through an entire hippocampus or anterior cortex. In brain, focal Vinculin was separated from diffuse cytosolic Vinculin by using the 'thresholding' function in ImageJ software, where the threshold was adjusted to convert the highest intensity signal from green to red while not altering the diffuse cytosolic Vinculin signal. The average area and size/puncta were quantitated with the ImageJ software. In primary neurons, vinculin immunoreactivity was quantified in dendrites and dendritic spines by subtracting diffuse cytosolic intensity in dendrites, which provides an internally controlled measure of focal vinculin *versus* diffuse cytosolic vinculin. All images were acquired with the Olympus FV10i confocal microscope and quantified using the Olympus Fluoview software (Olympus Corp.). All comparison images were acquired with identical laser intensity, exposure time, and filter. Adjustments to the brightness/contrast were applied equally to all comparison images.

JC-1, Mitosox-Red, and H2DCF imaging. HT22 cells seeded in 24-well plates were treated with/without HUTS-4 (1 : 250), MAB1965 (1 : 250), or Nox inhibitor III (40 nM) for 45 min, then treated with or without Aβ42$_O$ (1 μM) for 2 h. For Mitosox-Red imaging, cells were then washed with PBS and Mitosox-Red was added to a final concentration of 5 μM in PBS for 15 min at 37 °C, after which cells were washed with PBS, fixed, and imaged under the Olympus FV10i confocal microscope. For H2DCF imaging, after washing cells in PBS, H2DCF was added at a final concentration of 50 nM in HBSS for 15 min at 37 °C, followed by live-cell imaging at 37 °C with the Nikon Eclipse Ti fluorescence microscope (Nikon Instruments, Melville, NY, USA). For JC-1 imaging, after washing cells in PBS, JC-1 was added at a final concentration of 0.5 μM in PBS and incubated for 15 min at 37 °C, followed by live-cell imaging at 37 °C with the Nikon Eclipse Ti fluorescence microscope. All comparison images were acquired with identical laser or mercury lamp intensity, exposure time, and filter. Adjustments to the brightness/contrast were applied equally to all comparison images.

Stereotaxic surgery. Eight-month-old APP/PS1 mice were stereotaxically injected with 2 μl of either control IgG (control ascites diluted 1 : 10 in PBS) into the left hemisphere or β1-integrin neutralizing IgG (MAB1965 ascites diluted 1 : 10 in PBS) into the right hemisphere of the hippocampus (AP 2.7, Lat $-$2.7, DV $-$3.0) using the convection-enhanced delivery method described previously.[57] Forty-eight hours later, mice were subjected to transcardial perfusion with 4% paraformaldehyde followed by tissue sectioning and immunohistochemistry.

Electrophysiology in mouse brain slices. Hippocampus slices were prepared from 3-month-old WT, APP/PS1, and APP/PS1;*Cofilin*$^{+/-}$ mice and subjected to input/output curved, PPF, and LTP as previously described.[58] Briefly, animals were killed, and brains were harvested and sectioned horizontally (400 μm) in ice-cold cutting solution (110 mM sucrose, 6 mM NaCl, 3 mM KCl, 26 mM $NaHCO_3$, 1.25 mM NaH_2PO_4, 7 mM $MgCl_2$, 0.5 mM $CaCl_2$, and 10 g/l glucose, pH 7.3–7.4). The hippocampus was dissected and acclimated in 50:50 solution (cutting: artificial cerebrospinal fluid (ACSF)) for 10 min at room temperature. Further, the slices were transferred to ACSF (125 mM NaCl, 2.5 mM KCl, 1.25 mM NaH_2PO_4, 0.26 mM $NaHCO_3$, 1.2 mM $MgCl_2$, 2.0 mM $CaCl_2$, and 10 g/l glucose, pH 7.3–7.4, saturated with 95% O_2 and 5% CO_2). Slices were recovered in ACSF at room temperature at least 40 min, followed by a final incubation in ACSF for 1 h at 30 °C.

Extracellular field potential recording, LTP: The recording chamber was held at 30 $\pm$ 0.5 °C with ACSF flow rate of 1 ml/min. The stimulating electrode was placed in the Schaffer collaterals of the hippocampus. The recording glass electrode loaded with ACSF was positioned at the CA1 stratum radiatum below the pyramidal cell layer. Stimulating pulses were generated by the Digidata 1322 A interface (Molecular Devices, Sunnyvale, CA, USA) and a stimulus isolator (model 2200; A-M Systems, Sequim, WA, USA) under control of Clampex 10.0 software (Molecular Devices). Field excitatory postsynaptic potentials (fEPSPs) were amplified using a differential amplifier (model 1800; A-M Systems), filtered at 1 kHz, and digitized at 10 kHz.

Input–output curve was generated by stepping stimulation amplitude from 1 to 15 mV. Stimulation amplitude that elicited half-maximal fEPSP was determined by the input–output curve, and stimulation rate of 0.05 Hz was used through the whole experiment. PPF, which is short-term plasticity, was evoked by two pulses with interpulse intervals from 20 to 300 ms. Percentage of the facilitation was calculated by dividing fEPSP slope elicited by the second pulse with the fEPSP slope elicited by the first pulse. LTP was induced by TBS (five trains of four pulses at 200 Hz separated by 200 ms, repeated six times with an inter-train interval of 10 s). LTP was sampled 60 min after the induction, and calculated by dividing the slope of 60 min post-induction responses with the average slope of 20 min baseline responses.

Fear conditioning, open field, and rotarod behavior. Fear conditioning (contextual and cued), rotarod, and open-field tasks were performed as previously described.[59] For fear conditioning, an aversive stimulus (in this case a mild foot shock, 0.5 mA) was paired with an auditory conditioned stimulus (white noise) within a novel environment. Training consisted of two mild shocks paired with two conditioned stimuli with a 3-min interval between each shock. Freezing on the training day in response to the foot shock was used as an estimate of learning during the acquisition trial. To test conditioning to the context, animals were re-introduced to the same training chamber for 6 min and freezing behavior was recording by tracking software (Any-maze, Wood Dale, IL, USA) every second. To test conditioning to the tone, animals were introduced to a novel context, consisting of a chamber with different shape, floor, and olfactory cues from the training chamber. Mice were scored for 3 min, before and after the tone in the same manner described above. Learning was assessed by measuring freezing behavior (i.e., motionless position) every second. The open field was used as a standard test of general activity. Briefly, animals were monitored for 15 min in a 40-cm^2 open field with a video tracking software (Any-maze). General activity levels were evaluated by measurements of total distance traveled and total time immobile. Motor performance was evaluated by an accelerating rotarod apparatus with a 3-cm diameter rod starting at an initial rotation of 4 r.p.m. slowly accelerating to 40 r.p.m over 5 min. The time spent on the rod during each of four trials per day for 2 consecutive days was measured previously described in Brownlow *et al.*[60]

Statistical analysis and graphs. Statistical data were analyzed by the GraphPad Prism 6.0 software (GraphPad Software, San Diego, CA, USA) using Student's *t*-test, one- or two-way ANOVA. One- or two-way ANOVA was followed by Tukey *post hoc* test. All quantitative graphs were expressed as mean $\pm$ S.E.M. Differences were deemed significant when $P < 0.05$.

Conflict of Interest

The authors declare no conflict of interest.

Acknowledgements. This work was supported in part by NIH/NIA (1R01AG033055, DEK), NIH/NIA (1K02AG031920, DEK), and Florida Department of Health (5AZ07, DEK). We thank Dr. Elizabetta Bianchi for providing the RanBP9 monoclonal antibody.

1. Walsh DM, Klyubin I, Fadeeva JV, Cullen WK, Anwyl R, Wolfe MS *et al.* Naturally secreted oligomers of amyloid beta protein potently inhibit hippocampal long-term potentiation *in vivo*. *Nature* 2002; **416**: 535–539.
2. Selkoe DJ. Soluble oligomers of the amyloid beta-protein impair synaptic plasticity and behavior. *Behav Brain Res* 2008; **192**: 106–113.
3. Shankar GM, Bloodgood BL, Townsend M, Walsh DM, Selkoe DJ, Sabatini BL. Natural oligomers of the Alzheimer amyloid-beta protein induce reversible synapse loss by modulating an NMDA-type glutamate receptor-dependent signaling pathway. *J Neurosci* 2007; **27**: 2866–2875.
4. Zhao L, Ma QL, Calon F, Harris-White ME, Yang F, Lim GP *et al.* Role of p21-activated kinase pathway defects in the cognitive deficits of Alzheimer disease. *Nat Neurosci* 2006; **9**: 234–242.
5. Moreira PI, Santos MS, Moreno A, Oliveira C. Amyloid beta-peptide promotes permeability transition pore in brain mitochondria. *Biosci Rep* 2001; **21**: 789–800.
6. Du H, Guo L, Yan S, Sosunov AA, McKhann GM, Yan SS. Early deficits in synaptic mitochondria in an Alzheimer's disease mouse model. *Proc Natl Acad Sci USA* 2010; **107**: 18670–18675.
7. Minamide LS, Striegl AM, Boyle JA, Meberg PJ, Bamburg JR. Neurodegenerative stimuli induce persistent ADF/cofilin-actin rods that disrupt distal neurite function. *Nat Cell Biol* 2000; **2**: 628–636.
8. Kim T, Vidal GS, Djurisic M, William CM, Birnbaum ME, Garcia KC *et al.* Human LilrB2 is a beta-amyloid receptor and its murine homolog PirB regulates synaptic plasticity in an Alzheimer's model. *Science* 2013; **341**: 1399–1404.
9. Bernstein BW, Bamburg JR. ADF/cofilin: a functional node in cell biology. *Trends Cell Biol* 2010; **20**: 187–195.
10. Niwa R, Nagata-Ohashi K, Takeichi M, Mizuno K, Uemura T. Control of actin reorganization by Slingshot, a family of phosphatases that dephosphorylate ADF/cofilin. *Cell* 2002; **108**: 233–246.
11. Kurita S, Watanabe Y, Gunji E, Ohashi K, Mizuno K. Molecular dissection of the mechanisms of substrate recognition and F-actin-mediated activation of cofilin-phosphatase Slingshot-1. *J Biol Chem* 2008; **283**: 32542–32552.
12. Kim JS, Huang TY, Bokoch GM. Reactive oxygen species regulate a slingshot-cofilin activation pathway. *Mol Biol Cell* 2009; **20**: 2650–2660.
13. Roh SE, Woo JA, Lakshmana MK, Uhlar C, Ankala V, Boggess T *et al.* Mitochondrial dysfunction and calcium deregulation by the RanBP9-cofilin pathway. *FASEB J* 2013; **27**: 4776–4789.

14. Klamt F, Zdanov S, Levine RL, Pariser A, Zhang Y, Zhang B *et al.* Oxidant-induced apoptosis is mediated by oxidation of the actin-regulatory protein cofilin. *Nat Cell Biol* 2009; **11**: 1241–1246.
15. Bernstein BW, Shaw AE, Minamide LS, Pak CW, Bamburg JR. Incorporation of cofilin into rods depends on disulfide intermolecular bonds: implications for actin regulation and neurodegenerative disease. *J Neurosci* 2012; **32**: 6670–6681.
16. Becchetti A, Pillozzi S, Morini R, Nesti E, Arcangeli A. New insights into the regulation of ion channels by integrins. *Int Rev Cell Mol Biol* 2010; **279**: 135–190.
17. Zamir E, Geiger B. Molecular complexity and dynamics of cell-matrix adhesions. *J Cell Sci* 2001; **114**: 3583–3590.
18. Kim C, Ye F, Ginsberg MH. Regulation of integrin activation. *Annu Rev Cell Dev Biol* 2011; **27**: 321–345.
19. Lauren J, Gimbel DA, Nygaard HB, Gilbert JW, Strittmatter SM. Cellular prion protein mediates impairment of synaptic plasticity by amyloid-beta oligomers. *Nature* 2009; **457**: 1128–1132.
20. Um JW, Kaufman AC, Kostylev M, Heiss JK, Stagi M, Takahashi H *et al.* Metabotropic glutamate receptor 5 is a coreceptor for Alzheimer abeta oligomer bound to cellular prion protein. *Neuron* 2013; **79**: 887–902.
21. Wright S, Malinin NL, Powell KA, Yednock T, Rydel RE, Griswold-Prenner I. Alpha2beta1 and alphaVbeta1 integrin signaling pathways mediate amyloid-beta-induced neurotoxicity. *Neurobiol Aging* 2007; **28**: 226–237.
22. Wang Q, Klyubin I, Wright S, Griswold-Prenner I, Rowan MJ, Anwyl R. Alpha v integrins mediate beta-amyloid induced inhibition of long-term potentiation. *Neurobiol Aging* 2008; **29**: 1485–1493.
23. Dahlgren KN, Manelli AM, Stine WB Jr., Baker LK, Krafft GA, LaDu MJ. Oligomeric and fibrillar species of amyloid-beta peptides differentially affect neuronal viability. *J Biol Chem* 2002; **277**: 32046–32053.
24. Luque A, Gomez M, Puzon W, Takada Y, Sanchez-Madrid F, Cabanas C. Activated conformations of very late activation integrins detected by a group of antibodies (HUTS) specific for a novel regulatory region (355-425) of the common beta 1 chain. *J Biol Chem* 1996; **271**: 11067–11075.
25. Aljamal-Naylor R, Wilson L, McIntyre S, Rossi F, Harrison B, Marsden M *et al.* Allosteric modulation of beta1 integrin function induces lung tissue repair. *Adv Pharmacol Sci* 2012; **2012**: 768720.
26. Valdramidou D, Humphries MJ, Mould AP. Distinct roles of beta1 metal ion-dependent adhesion site (MIDAS), adjacent to MIDAS (ADMIDAS), and ligand-associated metal-binding site (LIMBS) cation-binding sites in ligand recognition by integrin alpha2beta1. *J Biol Chem* 2008; **283**: 32704–32714.
27. Raghavan S, Bauer C, Mundschau G, Li Q, Fuchs E. Conditional ablation of beta1 integrin in skin. Severe defects in epidermal proliferation, basement membrane formation, and hair follicle invagination. *J Cell Biol* 2000; **150**: 1149–1160.
28. Jankowsky JL, Fadale DJ, Anderson J, Xu GM, Gonzales V, Jenkins NA *et al.* Mutant presenilins specifically elevate the levels of the 42 residue beta-amyloid peptide in vivo: evidence for augmentation of a 42-specific gamma secretase. *Hum Mol Genet* 2004; **13**: 159–170.
29. Shirao T, Gonzalez-Billault C. Actin filaments and microtubules in dendritic spines. *J Neurochem* 2013; **126**: 155–164.
30. Eiseler T, Doppler H, Yan IK, Kitatani K, Mizuno K, Storz P. Protein kinase D1 regulates cofilin-mediated F-actin reorganization and cell motility through slingshot. *Nat Cell Biol* 2009; **11**: 545–556.
31. Jokinen J, White DJ, Salmela M, Huhtala M, Kapyla J, Sipila K *et al.* Molecular mechanism of alpha2beta1 integrin interaction with human echovirus 1. *EMBO J* 2010; **29**: 196–208.
32. Koenigsknecht J, Landreth G. Microglial phagocytosis of fibrillar beta-amyloid through a beta1 integrin-dependent mechanism. *J Neurosci* 2004; **24**: 9838–9846.
33. Pereira S, Zhang H, Takai T, Lowell CA. The inhibitory receptor PIR-B negatively regulates neutrophil and macrophage integrin signaling. *J Immunol* 2004; **173**: 5757–5765.
34. Loubet D, Dakowski C, Pietri M, Pradines E, Bernard S, Callebert J *et al.* Neuritogenesis: the prion protein controls beta1 integrin signaling activity. *FASEB J* 2012; **26**: 678–690.
35. Pantera B, Bini C, Cirri P, Paoli P, Camici G, Manao G *et al.* PrPc activation induces neurite outgrowth and differentiation in PC12 cells: role for caveolin-1 in the signal transduction pathway. *J Neurochem* 2009; **110**: 194–207.
36. Warren MS, Bradley WD, Gourley SL, Lin YC, Simpson MA, Reichardt LF *et al.* Integrin beta1 signals through Arg to regulate postnatal dendritic arborization, synapse density, and behavior. *J Neurosci* 2012; **32**: 2824–2834.
37. Babayan AH, Kramar EA, Barrett RM, Jafari M, Haettig J, Chen LY *et al.* Integrin dynamics produce a delayed stage of long-term potentiation and memory consolidation. *J Neurosci* 2012; **32**: 12854–12861.
38. Chan CS, Weeber EJ, Kurup S, Sweatt JD, Davis RL. Integrin requirement for hippocampal synaptic plasticity and spatial memory. *J Neurosci* 2003; **23**: 7107–7116.
39. Bernard-Trifilo JA, Kramar EA, Torp R, Lin CY, Pineda EA, Lynch G *et al.* Integrin signaling cascades are operational in adult hippocampal synapses and modulate NMDA receptor physiology. *J Neurochem* 2005; **93**: 834–849.
40. Rex CS, Chen LY, Sharma A, Liu J, Babayan AH, Gall CM *et al.* Different Rho GTPase-dependent signaling pathways initiate sequential steps in the consolidation of long-term potentiation. *J Cell Biol* 2009; **186**: 85–97.
41. Zhou Q, Homma KJ, Poo MM. Shrinkage of dendritic spines associated with long-term depression of hippocampal synapses. *Neuron* 2004; **44**: 749–757.
42. Chen LY, Rex CS, Casale MS, Gall CM, Lynch G. Changes in synaptic morphology accompany actin signaling during LTP. *J Neurosci* 2007; **27**: 5363–5372.
43. Gu J, Lee CW, Fan Y, Komlos D, Tang X, Sun C *et al.* ADF/cofilin-mediated actin dynamics regulate AMPA receptor trafficking during synaptic plasticity. *Nat Neurosci* 2010; **13**: 1208–1215.
44. Pontrello CG, Sun MY, Lin A, Fiacco TA, DeFea KA, Ethell IM. Cofilin under control of beta-arrestin-2 in NMDA-dependent dendritic spine plasticity, long-term depression (LTD), and learning. *Proc Natl Acad Sci USA* 2012; **109**: E442–E451.
45. Werner E, Werb Z. Integrins engage mitochondrial function for signal transduction by a mechanism dependent on Rho GTPases. *J Cell Biol* 2002; **158**: 357–368.
46. Walsh KP, Minamide LS, Kane SJ, Shaw AE, Brown DR, Pulford B *et al.* Amyloid-beta and proinflammatory cytokines utilize a prion protein-dependent pathway to activate NADPH oxidase and induce cofilin-actin rods in hippocampal neurons. *PloS One* 2014; **9**: e95995.
47. Boyd-Kimball D, Sultana R, Poon HF, Lynn BC, Casamenti F, Pepeu G *et al.* Proteomic identification of proteins specifically oxidized by intracerebral injection of amyloid beta-peptide (1-42) into rat brain: implications for Alzheimer's disease. *Neuroscience* 2005; **132**: 313–324.
48. Sultana R, Newman SF, Abdul HM, Cai J, Pierce WM, Klein JB *et al.* Protective effect of D609 against amyloid-beta1-42-induced oxidative modification of neuronal proteins: redox proteomics study. *J Neurosci Res* 2006; **84**: 409–417.
49. Mendoza-Naranjo A, Contreras-Vallejos E, Henriquez DR, Otth C, Bamburg JR, Maccioni RB *et al.* Fibrillar amyloid-beta1-42 modifies actin organization affecting the cofilin phosphorylation state: a role for Rac1/cdc42 effector proteins and the slingshot phosphatase. *J Alzheimer's Dis* 2012; **29**: 63–77.
50. Wang Y, Shibasaki F, Mizuno K. Calcium signal-induced cofilin dephosphorylation is mediated by Slingshot via calcineurin. *J Biol Chem* 2005; **280**: 12683–12689.
51. Woo JA, Jung AR, Lakshmana MK, Bedrossian A, Lim Y, Bu JH *et al.* Pivotal role of the RanBP9-cofilin pathway in Abeta-induced apoptosis and neurodegeneration. *Cell Death Differ* 2012; **19**: 1413–1423.
52. Liu T, Roh SE, Woo JA, Ryu H, Kang DE. Cooperative role of RanBP9 and P73 in mitochondria-mediated apoptosis. *Cell Death Dis* 2013; **4**: e476.
53. Humphries JD, Wang P, Streuli C, Geiger B, Humphries MJ, Ballestrem C. Vinculin controls focal adhesion formation by direct interactions with talin and actin. *J Cell Biol* 2007; **179**: 1043–1057.
54. Soriano S, Kang DE, Fu M, Pestell R, Chevallier N, Zheng H *et al.* Presenilin 1 negatively regulates beta-catenin/T cell factor/lymphoid enhancer factor-1 signaling independently of beta-amyloid precursor protein and notch processing. *J Cell Biol* 2001; **152**: 785–794.
55. Kang DE, Soriano S, Xia X, Eberhart CG, De SB, Zheng H *et al.* Presenilin couples the paired phosphorylation of beta-catenin independent of axin: implications for beta-catenin activation in tumorigenesis. *Cell* 2002; **110**: 751–762.
56. Lakshmana MK, Yoon IS, Chen E, Bianchi E, Koo EH, Kang DE. Novel role of RanBP9 in BACE1 processing of amyloid precursor protein and amyloid beta peptide generation. *J Biol Chem* 2009; **284**: 11863–11872.
57. Carty N, Lee D, Dickey C, Ceballos-Diaz C, Jansen-West K, Golde TE *et al.* Convection-enhanced delivery and systemic mannitol increase gene product distribution of AAV vectors 5, 8, and 9 and increase gene product in the adult mouse brain. *J Neurosci Methods* 2010; **194**: 144–153.
58. Weeber EJ, Beffert U, Jones C, Christian JM, Forster E, Sweatt JD *et al.* Reelin and ApoE receptors cooperate to enhance hippocampal synaptic plasticity and learning. *J Biol Chem* 2002; **277**: 39944–39952.
59. Bolognani F, Qiu S, Tanner DC, Paik J, Perrone-Bizzozero NI, Weeber EJ. Associative and spatial learning and memory deficits in transgenic mice overexpressing the RNA-binding protein HuD. *Neurobiol Learn Mem* 2007; **87**: 635–643.
60. Brownlow ML, Benner L, D'Agostino D, Gordon MN, Morgan D. Ketogenic diet improves motor performance but not cognition in two mouse models of Alzheimer's pathology. *PloS One* 2013; **8**: e75713.

Supplementary Information accompanies this paper on Cell Death and Differentiation website (http://www.nature.com/cdd)